Inorganic Chemistry
Cite This: Inorg. Chem. 2018, 57, 1158−1170
Article
pubs.acs.org/IC

Understanding the Mechanism of Magnetic Relaxation in Pentanuclear $\{Mn^{IV}Mn^{III}_2Ln^{III}_2\}$ Single-Molecule Magnets

Kuduva R. Vignesh,[†] Stuart K. Langley,[‡] Boujemaa Moubaraki,[§] Keith S. Murray,*[,§] and Gopalan Rajaraman*[,∥]

[†]IITB-Monash Research Academy, IIT Bombay, Mumbai 400076, India
[‡]School of Science and the Environment, Division of Chemistry, Manchester Metropolitan University, Manchester, U.K.
[§]School of Chemistry, 17 Rainforest Walk, Monash University, Clayton, Victoria 3800, Australia
[∥]Department of Chemistry, IIT Bombay, Mumbai 400076, India

Supporting Information

ABSTRACT: A new family of heterometallic pentanuclear complexes of formulas $[Mn^{IV}Mn^{III}_2Ln^{III}_2O_2(benz)_4(mdea)_3(NO_3)_2(MeOH)]$ (Ln = Dy (**1-Dy**), Tb (**2-Tb**), Gd (**3-Gd**), Eu (**4-Eu**), Sm (**5-Sm**), Nd (**6-Nd**), Pr (**7-Pr**); benz(H) = benzoic acid; $mdeaH_2$= *N*-methyldiethanolamine) and $[Mn^{IV}Mn^{III}_2Ln^{III}_2O_2(o\text{-tol})_4(mdea)_3(NO_3)_2(MeOH)]$ (Ln = Gd (**8-Gd**), Eu (**9-Eu**); *o*-tol(H) = *o*-toluic acid) have been isolated and structurally, magnetically, and theoretically characterized. dc magnetic susceptibility measurements reveal dominant antiferromagnetic magnetic interactions for each complex, except for **2-Tb** and **3-Gd**, which reveal an upturn in the $\chi_M T$ product at low temperatures. The magnetic interactions between the spin centers in the Gd derivatives, **3-Gd** and **8-Gd**, which display markedly different $\chi_M T$ vs T profiles, were found to be due to the interactions of the Gd^{III}−Gd^{III} ions which change from ferromagnetic (**3-Gd**) to antiferromagnetic (**8-Gd**) due to structural differences. ac magnetic susceptibility measurements reveal a nonzero out-of-phase component for **1-Dy** and **7-Pr**, but no maxima were observed above 2 K (H_{dc} = 0 Oe), which suggests single-molecule magnet (SMM) behavior. Out-of-phase signals were observed for complexes **2-Tb**, **4-Eu**, **8-Gd**, and **9-Eu**, in the presence of a static dc field (H_{dc} = 2000, 3000 Oe). The anisotropic nature of the lanthanide ions in the benzoate series (**1-Dy**, **2-Tb**, **5-Sm**, **6-Nd**, and **7-Pr**) were thoroughly investigated using ab initio methods. CASSCF calculations predict that the origin of SMM behavior in **1-Dy** and **7-Pr** and the applied field SMM behavior in **2-Tb** does not solely originate from the single-ion anisotropy of the lanthanide ions. To fully understand the relaxation mechanism, we have employed the Lines model to fit the susceptibility data using the POLY_ANISO program, which suggests that the zero-field SMM behavior observed in complexes **1-Dy** and **7-Pr** is due to weak $Mn^{III/IV}$−Ln^{III} and Ln^{III}−Ln^{III} couplings and an unfavorable $Ln^{III}/Mn^{III}/Mn^{IV}$ anisotropy. In complexes **4-Eu**, **8-Gd**, and **9-Eu** ab initio calculations indicate that the anisotropy of the Mn^{III} ions solely gives rise to the possibility of SMM behavior. Complex **7-Pr** is a Pr(III)-containing complex that displays zero-field SMM behavior, which is rare, and our study suggests the possibility of coupling weak SOC lanthanide metal ions to anisotropic transition-metal ions to derive SMM characteristics; however, enhancing the exchange coupling in {3d−4f} complexes is still a stubborn hurdle in harnessing new generation {3d−4f} SMMs.

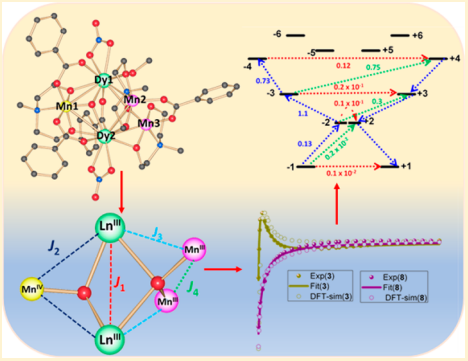

INTRODUCTION

Since the report of the first single-molecule magnet (SMM), $\{Mn_{12}$-acetate$\}$,[1] great efforts have been made in the construction of new SMM materials. These molecular materials have potential applications in high-density information storage devices,[2] Q-bits,[3] and "Spintronic" devices.[3a,4] Prerequisites for SMM behavior include a high-spin ground state (S) with negative zero field splitting (D), and when these two properties are observed, this leads to slow relaxation of the magnetization, purely of molecular origin, usually at very low temperatures (<5 K).[5] The energy barrier for magnetic reorientation (U_{eff}) is correlated to these aforementioned parameters. SMM behavior is exhibited in certain mono- and polynuclear metal ion complexes, and initial efforts[2] focused on isolating large transition-metal coordination complexes with significant spin (S) ground states.[6] At the same time, strongly anisotropic transition-metal ions are also included in the molecular aggregates to enhance the magnetic anisotropy.[6,7] These efforts led to large barrier heights (U_{eff}) being observed in several polynuclear complexes, including hexanuclear $\{Mn_6\}$ species.[8] Other cluster species, such as $\{Mn_{19}\}$, which possesses an unusually large molecular spin ground state of S = 83/2,[6] does not display any SMM behavior due to a lack of anisotropy. This result has also been found for the majority of high-spin metal complexes.[6,7b,9] Following these observations, greater attention has been paid to

Received: October 10, 2017
Published: January 8, 2018

DOI: 10.1021/acs.inorgchem.7b02608
Inorg. Chem. 2018, 57, 1158−1170

modulate magnetic anisotropy in SMMs, with lanthanide-based SMMs taking center stage.[10]

Among the lanthanide ions, Dy^{III} and Tb^{III} have been the most prolific with numerous SMM examples,[11] including a Dy^{III} SMM exhibiting a blocking temperature (magnetic relaxation of 100 s) of 12 K, with hysteresis open up to 30 K[12] (sweep rate 20 mT s^{-1}) and a blocking temperature of 60 K for a Dy^{III} organometallic SMM.[13] Unlike the case with transition-metal ions, the magnetic ground state(s) for lanthanide ion complexes are characterized by their corresponding m_J levels, and the splitting between the m_J levels, due to crystal field interaction, can be correlated to the zero-field splitting parameter in transition-metal complexes. Lanthanide ions, despite possessing a large magnetic anisotropy, however, in general, exhibit a loss of magnetization at zero magnetic field and thus low hysteretic blocking temperatures are observed (with several important exceptions[12,13]). This is essentially due to dominant quantum tunneling of magnetization (QTM) due to large spin−orbit coupling (SOC) and low-symmetry environments. One way to quench QTM for lanthanide SMMs includes the incorporation of organic radical species or 3d metal ions in Ln complex aggregation to enable stronger magnetic exchange coupling between the radical/3d ion with the 4f ions. Within radical-based 4f systems, a $[Tb_2(\mu\text{-}N_2^{3-})]$ example is worthy of mention, as this is reported to possess a U_{eff} value of 326 K, with magnetic hysteresis observed at 14 K,[14] arising due to very strong radical−4f magnetic exchange.[15] However, radical-based 4f complexes are often unstable under ambient conditions and incorporation of 3d elements along with 4f is therefore a viable alternative. Thus, heterometallic 3d−4f complexes have gained attention, as they possess a combination of a large spin on the 3d ions with the spin/anisotropy of lanthanide ions.[16] Several 3d−4f clusters such as $\{Dy_4Mn_{11}\}$,[16d] $\{Mn_6Tb_2\}$,[16e] $\{Dy^{III}{}_2Co^{III}{}_2\}$,[16a−e] and $\{Dy^{III}{}_2Cr^{III}{}_2\}$[17] are reported to possess SMM behavior. In particular, the "butterfly" type complexes $\{Co^{III}{}_2Dy^{III}{}_2\}$[16a−e] and $\{Cr^{III}{}_2Dy^{III}{}_2\}$,[17] reported by some of us, highlight the important role the magnetic exchange interaction plays in quenching QTM, leading to considerably longer relaxation times with highly coercive hysteresis loops in the $\{Cr^{III}{}_2Dy^{III}{}_2\}$ family.[17] For the construction of $\{Dy^{III}{}_2Co^{III}{}_2\}$[16a−c] and $\{Dy^{III}{}_2Cr^{III}{}_2\}$[17] type complexes the common ligand(s) used in their synthesis are amine polyalcohol ligands such as triethanolamine ($teaH_3$) and *N*-methyldiethanolamine ($mdeaH_2$). Moreover, these ligands have led to the isolation of an attractive 16-membered heterometallic $\{Mn^{III}-Ln^{III}\}$ wheel using Mn^{III} as the 3d ion[18] and a six-membered Dy^{III}−metallo wheel; the latter shows a rare net toroidal magnetic moment as a single-molecule toroic.[19]

In this work, we target new heterometallic complexes and have focused on the use of Mn^{III} ion with anisotropic Ln^{III} ions. We report the synthesis of a family of pentanuclear $\{Mn^{IV}Mn^{III}{}_2Ln^{III}{}_2\}$ complexes of formula $[Mn^{IV}Mn^{III}{}_2Ln^{III}{}_2O_2(RCO_2)_4(mdea)_3(NO_3)_2(MeOH)]$ (Ln = Dy (**1-Dy**), Tb (**2-Tb**), Gd (**3-Gd** and **8-Gd**), Eu (**4-Eu** and **9-Eu**), Sm (**5-Sm**), Nd (**6-Nd**) and Pr (**7-Pr**), where $mdea^{2-}$ = doubly deprotonated *N*-methyldiethanolamine, RCO_2^- = benzoate (**1-Dy** to **7-Pr**) or toluate (**8-Gd** and **9-Eu**)) and have performed magnetic measurements on these compounds and interpreted the data using various theoretical techniques.

EXPERIMENTAL SECTION

General Information. All reactions were carried out under aerobic conditions. Chemicals and solvents were obtained from commercial sources and used without further purification.

Synthesis of Metal Complexes. *Synthesis of $[Mn^{IV}Mn^{III}{}_2Dy^{III}{}_2O_2(benz)_4(mdea)_3(NO_3)_2(MeOH)]$ (**1-Dy**).* $Mn(NO_3)_2{\cdot}4H_2O$ (0.288 g, 1 mmol) and $Dy(NO_3)_3{\cdot}6H_2O$ (0.22 g, 0.5 mmol) were dissolved in MeCN (20 mL), followed by the addition of *N*-methyldiethanolamine (0.1 mL, 1 mmol), benzoic acid (0.12 g, 1.0 mmol), and triethylamine (0.55 mL, 4.0 mmol), which resulted in a brown solution. This solution was stirred for 2 h, after which the solvent was removed to give a brown oil. The oil was redissolved in MeOH/EtOH (1/1) and layered with diethyl ether (Et_2O). Within 5−7 days, dark brown crystals of **1-Dy** had appeared, with an approximate yield of 45% (crystalline product). Anal. Calcd (found) for **1-Dy**, $Mn_3Dy_2C_{44}H_{57}O_{23}N_5$: C, 34.91 (34.65); H, 3.80 (3.87); N, 4.63 (4.64).

*Synthesis of $[Mn^{IV}Mn^{III}{}_2Tb^{III}{}_2O_2(benz)_4(mdea)_3(NO_3)_2(MeOH)]$ (**2-Tb**).* The synthetic route for **1-Dy** was followed, but $Tb(NO_3)_3{\cdot}6H_2O$ (0.17 g, 0.5 mmol) was used in place of $Dy(NO_3)_3{\cdot}6H_2O$. Dark brown crystals of **2-Tb** appeared within 7−8 days, with an approximate yield of 47% (crystalline product). Anal. Calcd (found) for **2-Tb**, $Mn_3Tb_2C_{44}H_{57}O_{23}N_5$: C, 35.08 (35.11); H, 3.81 (3.57); N, 4.65 (4.81).

*Synthesis of $[Mn^{IV}Mn^{III}{}_2Gd^{III}{}_2O_2(benz)_4(mdea)_3(NO_3)_2(MeOH)]$ (**3-Gd**).* The synthetic route for **1-Dy** was followed, but $Gd(NO_3)_3{\cdot}6H_2O$ (0.22 g,0.5 mmol) was used in place of $Dy(NO_3)_3{\cdot}6H_2O$. Dark brown crystals of **3-Gd** appeared within 3−4 days, with an approximate yield of 55% (crystalline product). Anal. Calcd (found) for **3-Gd**, $Mn_3Dy_2C_{44}H_{57}O_{23}N_5$: C, 35.16 (34.89); H, 3.81 (3.57); N, 4.65 (4.44).

*Synthesis of $[Mn^{IV}Mn^{III}{}_2Eu^{III}{}_2O_2(benz)_4(mdea)_3(NO_3)_2(MeOH)]$ (**4-Eu**).* The synthetic route for **1-Dy** was followed, but $Eu(NO_3)_3{\cdot}xH_2O$ (0.17 g, 0.5 mmol) was used in place of $Dy(NO_3)_3{\cdot}6H_2O$. Dark brown crystals of **4-Eu** appeared within 5−7 days, with an approximate yield of 50% (crystalline product). Anal. Calcd (found) for **4-Eu**, $Mn_3Eu_2C_{44}H_{57}O_{23}N_5$: C, 35.40 (35.87); H, 3.85 (3.59); N, 4.69 (4.77).

*Synthesis of $[Mn^{IV}Mn^{III}{}_2Sm^{III}{}_2O_2(benz)_4(mdea)_3(NO_3)_2(MeOH)]$ (**5-Sm**).* The synthetic route for **1-Dy** was followed, but $Sm(NO_3)_3{\cdot}6H_2O$ (0.22 g, 0.5 mmol) was used in place of $Dy(NO_3)_3{\cdot}6H_2O$. Dark brown crystals of **5-Sm** appeared within 8−10 days, with an approximate yield of 55% (crystalline product). Anal. Calcd (found) for **5-Sm**, $Mn_3Sm_2C_{44}H_{57}O_{23}N_5$: C, 35.48 (35.45); H, 3.86 (3.87); N, 4.70 (4.99).

*Synthesis of $[Mn^{IV}Mn^{III}{}_2Nd^{III}{}_2O_2(benz)_4(mdea)_3(NO_3)_2(MeOH)]$ (**6-Nd**).* The synthetic route for **1-Dy** was followed, but $Nd(NO_3)_3{\cdot}6H_2O$ (0.22 g, 0.5 mmol) was used in place of $Dy(NO_3)_3{\cdot}6H_2O$. Dark brown crystals of **6-Nd** appeared within 3−4 days, with an approximate yield of 65% (crystalline product). Anal. Calcd (found) for **6-Nd**, $Mn_3Nd_2C_{44}H_{57}O_{23}N_5$: C, 35.77 (35.46); H, 3.89 (3.56); N, 4.74 (4.64).

*Synthesis of $[Mn^{IV}Mn^{III}{}_2Pr^{III}{}_2O_2(benz)_4(mdea)_3(NO_3)_2(MeOH)]$ (**7-Pr**).* The synthetic route for **1-Dy** was followed, but $Pr(NO_3)_3{\cdot}6H_2O$ (0.22 g, 0.5 mmol) was used in place of $Dy(NO_3)_3{\cdot}6H_2O$. Dark brown crystals of **7-Pr** appeared within 5−7 days, with an approximate yield of 45% (crystalline product). Anal. Calcd (found) for **7-Pr**, $Mn_3Pr_2C_{44}H_{57}O_{23}N_5$: C, 35.94 (35.85); H, 3.91 (3.69); N, 4.76 (4.64).

*Synthesis of $[Mn^{IV}Mn^{III}{}_2Gd^{III}{}_2O_2(o\text{-}tol)_4(mdea)_3(NO_3)_2(MeOH)]{\cdot}3H_2O$ (**8-Gd**).* The synthetic route for **3-Gd** was followed, but *o*-toluic acid (0.14 g, 0.5 mmol) was used in place of benzoic acid. Dark brown crystals of **8-Gd** appeared within 3−4 days, with an approximate yield of 57% (crystalline product). Anal. Calcd (found) for **8-Gd**, $Mn_3Gd_2C_{48}H_{71}O_{26}N_5$: C, 35.73 (35.25); H, 4.44 (4.87); N, 4.34 (4.55).

*Synthesis of $[Mn^{IV}Mn^{III}{}_2Eu^{III}{}_2O_2(o\text{-}tol)_4(mdea)_3(NO_3)_2(MeOH)]{\cdot}3H_2O$ (**9-Eu**).* The synthetic route for **8-Gd** was followed but, $Eu(NO_3)_3{\cdot}xH_2O$ (0.17 g, 0.5 mmol) was used in place of $Gd(NO_3)_3{\cdot}6H_2O$. Dark brown crystals of **9-Eu** appeared within 8−10 days, with an approximate yield of 54% (crystalline product). Anal. Calcd (found) for **9-Eu**, $Mn_3Eu_2C_{48}H_{71}O_{26}N_5$: C, 35.97 (35.75); H, 4.46 (4.57); N, 4.37 (4.34).

X-ray Crystallography. X-ray measurements for **1-Dy**−**5-Sm** and **9-Eu** were performed at 100(2) K at the Australian synchrotron MX1 beamline.[20] The data collection and integration were performed within Blu-Ice[21] and XDS[22] software programs. Data collection and integration were performed with SMART and SAINT+ software programs and corrected for absorption using the Bruker SADABS program. Compounds **1-Dy** to **5-Sm** and **9-Eu** were solved by direct methods (SHELXS-97)[23] and refined (SHELXL-97)[24] by full-matrix least squares on all F^2 data.[25] The crystallographic data and refinement parameters of **1-Dy** to **5-Sm** and **9-Eu** are summarized in Table S1 in the

DOI: 10.1021/acs.inorgchem.7b02608
Inorg. Chem. 2018, 57, 1158−1170

Supporting Information. Crystallographic details are available as CCDC numbers 1571429−1571434. X-ray powder diffraction patterns for complexes **6-Nd, 7-Pr**, and **8-Gd** were measured on a Bruker X8 instrument using Cu Kα radiation (1.5418 Å), and the samples were mounted on a zero-background silicon single-crystal stage. Scans were performed at room temperature in the 2θ range of 5−55° and compared with predicted patterns that were based on low-temperature single-crystal data.

Magnetic Measurements. Magnetic susceptibility measurements were carried out on a Quantum Design MPMS-XL 7 SQUID magnetometer that operated between 1.8 and 300 K for dc applied fields that ranged from 0 to 5 T. Microcrystalline samples were dispersed in Vaseline in order to avoid torquing of the crystallites. The sample mulls were contained in a calibrated gelatin capsule that was held at the center of a drinking straw that was fixed at the end of the sample rod. Alternating current (ac) susceptibilities were carried out under an oscillating ac field of 3.5 Oe, with frequencies ranging from 0.1 to 1500 Hz.

Computational Details. *DFT Calculations.* DFT calculations, combined with the broken-symmetry (BS) approach,[26] have been employed to compute the J values in complexes **3-Gd** and **8-Gd** (modeled using X-ray structure of **9-Eu**). The BS method has a proven record of yielding good numerical estimates of J constants for a variety of complexes[27] such as dinuclear transition-metal complexes[28] and Gd-based di-[15a,29] and polynuclear complexes.[9c,18,27a,30] Here DFT calculations were performed using the B3LYP functional[31] with the Gaussian 09 suite of programs.[32] In complexes **3-Gd** and **8-Gd**, the double-ζ quality basis set that employed a Cundari−Stevens (CS) relativistic effective core potential on Gd atom[33] and Ahlrich's[34] triple-ζ-quality basis set were employed for Mn and the rest of the atoms. The following Hamiltonian was used to estimate the exchange interaction (J):

$$\hat{H} = -[2J_1(S_{Gd1}S_{Gd2}) + 2J_2(S_{Gd1}S_{Mn3} + S_{Gd2}S_{Mn3}) + 2J_3(S_{Gd1}S_{Mn4} + S_{Gd2}S_{Mn5}) + 2J_4(S_{Mn4}S_{Mn5}) \quad (1)$$

The computed energies of five spin configurations for **3-Gd** and **8-Gd** were used to extract the exchange interactions.[35] The PHI program[36] was used for the simulation of plots of magnetic susceptibilities vs temperature and for molar magnetization vs field for **3-Gd** and **8-Gd**.

Ab Initio Calculations. Using MOLCAS 8.0,[37] ab initio calculations were performed on the mononuclear Ln ions of complexes **1-Dy**, **2-Tb**, **5-Sm**, **6-Nd**, and **7-Pr**. We have used the X-ray crystal structures of **1-Dy**, **2-Tb**, and **5-Sm** for their calculations, and the X-ray structure of **5-Sm** has been used to model **6-Nd** and **7-Pr** for their calculations. The neighboring Ln^{III}, Mn^{IV}, and Mn^{III} ions were replaced by diamagnetic Lu^{III}, Ti^{IV}, and Ga^{III}, respectively, in the calculation. The relativistic effects are taken into account on the basis of the Douglas−Kroll Hamiltonian.[38] The spin-free eigenstates were achieved by the complete active space self-consistent field (CASSCF) method.[39] We have employed the [ANO-RCC···8s7p5d3f2g1h] basis set[40] for Ln atoms, the [ANO-RCC···3s2p] basis set for C atoms, the [ANO-RCC···2s] basis set for H atoms, the [ANO-RCC···3s2p1d] basis set for N atoms, the [ANO-RCC···4s3p1d] basis set for Ga atoms, the [ANO-RCC···7s6p4d2f] basis set for the Lu atom, and the [ANO-RCC···3s2p1d] basis set for O atoms. First, the CASSCF calculations were performed by including nine electrons across seven 4f orbitals of the Dy^{III} ion for **1-Dy**, eight electrons across seven 4f orbitals of the Tb^{III} ion for **2-Tb**, five electrons across seven 4f orbitals of the Sm^{III} ion for **5-Sm**, four electrons across seven 4f orbitals of the Nd^{III} ion for **6-Nd**, and three electrons across seven 4f orbitals of the Pr^{III} ion for **7-Pr**. With this active space, 21 roots of sextet in the configuration interaction (CI) procedure were computed for **1-Dy**. For **2-Tb**, 7 septet excited states, 140 quintet excited states, and 195 triplet excited states were considered. For **5-Sm**, 21 sextet excited states, 128 quartet excited states, and 130 doublet excited states were considered. For **6-Nd**, 35 quartet excited states and 112 doublet excited states were considered. For **7-Pr**, 21 triplet excited states and 28 singlet excited states were considered. After computing these excited states, we mixed all roots using the RASSI-SO procedure;[41] spin−orbit coupling has been considered within the space of the calculated spin-free eigenstates. Moreover, these computed SO states have been considered in the SINGLE_ANISO[42] program to compute the **g** tensors. The Cholesky decomposition for two-electron integrals is employed throughout our calculations. The crystal field parameters have been extracted using the SINGLE_ANISO code, as implemented in MOLCAS 8.0. The exchange interactions of anisotropic Ln ions and Mn^{III}−Ln^{III}, Mn^{IV}−Ln^{III}, and Mn^{III}−Mn^{III} interactions in complexes **1-Dy**, **2-Tb**, **5-Sm**, **6-Nd**, and **7-Pr** have been computed by fitting with the experimental data using the POLY_ANISO[43] routine employing Lines model.[44]

The magnetic couplings were extracted using the Hamiltonian

$$\hat{H}_{ex} = -\sum_{i=1}^{3} J_i \cdot S_i \cdot S_{i+1} \quad (2)$$

(here $J_i = J_i^{dipolar} + J_i^{exch}$, i.e. J_i values are the total magnetic interactions in combination of calculated $J_i^{dipolar}$ and fitted J_i^{exch} parameters; this describes the interaction between the intramolecular metal centers)

To calculate the **D** tensor for a Mn^{IV} ion and both Mn^{III} ions in **1-Dy**, ab initio CASSCF calculations were performed using MOLCAS 8.0.[37] The active space for CASSCF calculations comprises five d-based orbitals with three electrons for the Mn^{IV} ion in the CAS(3,5) setup and four electrons for Mn^{III} ions in the CAS(4,5) setup. We then considered 10 quartet and 40 doublet excited states for the Mn^{IV} ion and 5 quintet and 40 five triplet excited states for the Mn^{III} ion in the calculations in order to compute zero field splitting (zfs).[45] After computing these excited states, we mixed all roots using RASSI-SO[41] and computed the **D** tensor using the SINGLE_ANISO[42] program.

RESULTS AND DISCUSSION

Synthesis and Crystal Structures. The reaction of $Mn(NO_3)_2{\cdot}4H_2O$ and $Ln(NO_3)_3{\cdot}6H_2O$ (Ln = Dy, Tb, Gd, Eu, Sm, Nd, Pr) with $mdeaH_2$ and benzoic acid or *o*-toluic acid in acetonitrile at ambient temperature, followed by the removal of the solvent and redissolution in a MeOH/EtOH mixture, yielded a family of mixed-valent heterometallic pentanuclear complexes of general formula $[Mn^{IV}Mn^{III}{}_2Ln^{III}{}_2O_2(benz)_4(mdea)_3(NO_3)_2(MeOH)]$ (Ln = Dy (**1-Dy**), Tb (**2-Tb**), Gd (**3-Gd**), Eu (**4-Eu**), Sm (**5-Sm**), Nd (**6-Nd**), Pr (**7-Pr**)) or $[Mn^{IV}Mn^{III}{}_2Ln^{III}{}_2O_2(o\text{-tol})_4(mdea)_3(NO_3)_2(MeOH)]{\cdot}3H_2O$ (Ln = Gd (**8-Gd**) and Eu (**9-Eu**)) (see Scheme 1). We note that it is also possible to isolate a $\{Mn^{III}{}_2Ln^{III}{}_2\}$ "reverse butterfly" motif using these ligands (similar to the conventional $\{Co^{III}{}_2Dy^{III}{}_2\}$ and $\{Cr^{III}{}_2Dy^{III}{}_2\}$ butterfly complexes highlighted above,[16a−c,17]) when MeOH was used as the crystallization solvent.[46] For all complexes, it is interesting to note that by modifying the crystallization solvent (MeOH/EtOH) a different complex is isolated. Furthermore, we find that the above pentanuclear products are sensitive to the lanthanide ion used and can only be isolated for Ln^{III} ions up to Dy^{III} in the 4f block. When Ln^{III} ions of atomic number greater than Dy^{III} are used, we find that a new product is isolated under the same crystallization conditions: namely, a $[Mn^{III}{}_8Ln^{III}{}_8(mdea)_{16}(o\text{-tol})_8(NO_3)_8]$ (Ln = Dy^{III}−Yb^{III}) wheel complex.[18] While it is always difficult to predict/rationalize the structure of the solid-state product when a self-assembly approach is used, it is clear that the nature of the lanthanide ion, likely the ionic radii of the ions, and solvent effects play significant roles in the outcome of these reactions.

Compounds **1-Dy** to **5-Sm** and **9-Eu** crystallize in the triclinic space group $P\bar{1}$, such that the asymmetric unit constitutes the entire molecule (see Figure 1). The solid-state structures of **6-Nd**, **7-Pr**, and **8-Gd** were determined by their powder XRD diffraction patterns, where the PXRD suggests the possibility that **6-Nd** and **7-Pr** are identical with those simulated from the Sm compound **5-Sm**, while that for complex **8-Gd** is identical to the simulated pattern for the Eu compound **9** (Figure 2).

DOI: 10.1021/acs.inorgchem.7b02608
Inorg. Chem. 2018, 57, 1158−1170

Scheme 1. Reaction Scheme Used To Isolate Compounds 1-Dy to 7-Pr (R = H) and 8-Gd and 9-Eu (R = Me)

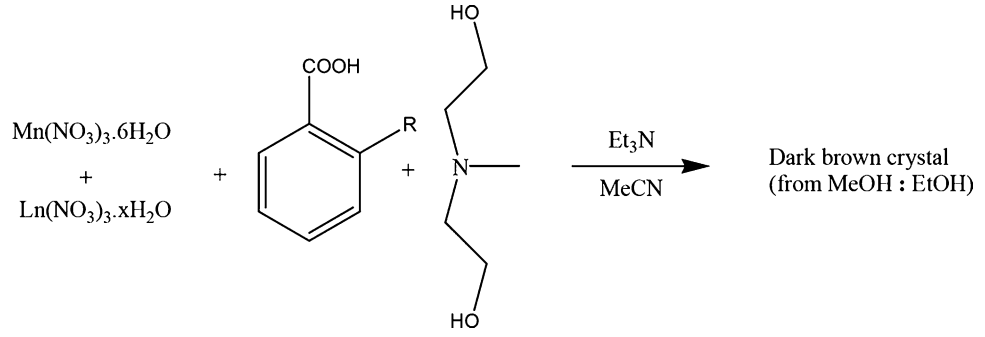

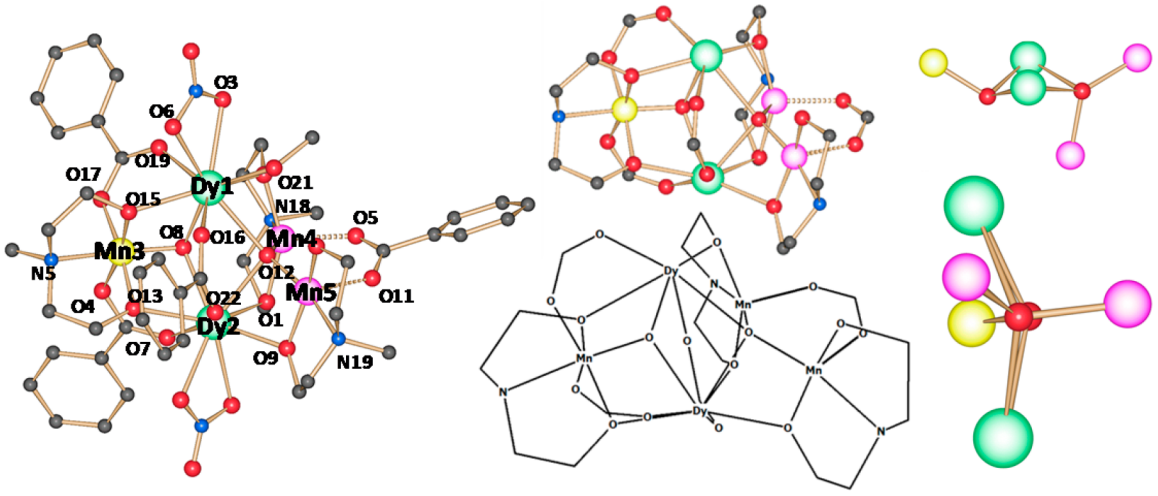

Figure 1. (left) Molecular structure of complex **1-Dy**. The solvent and the H atoms are omitted for clarity. The dotted bonds indicate the elongated axis. Color scheme: Mn^{IV}, yellow; Mn^{III}, pink; Dy^{III}, green; O, red; N, blue; C, light gray. (middle) Simplified molecular structure of ChemDraw type of **1-Dy** showing bridging connectivity. (right) Core structure of complex **1-Dy** with top and side views.

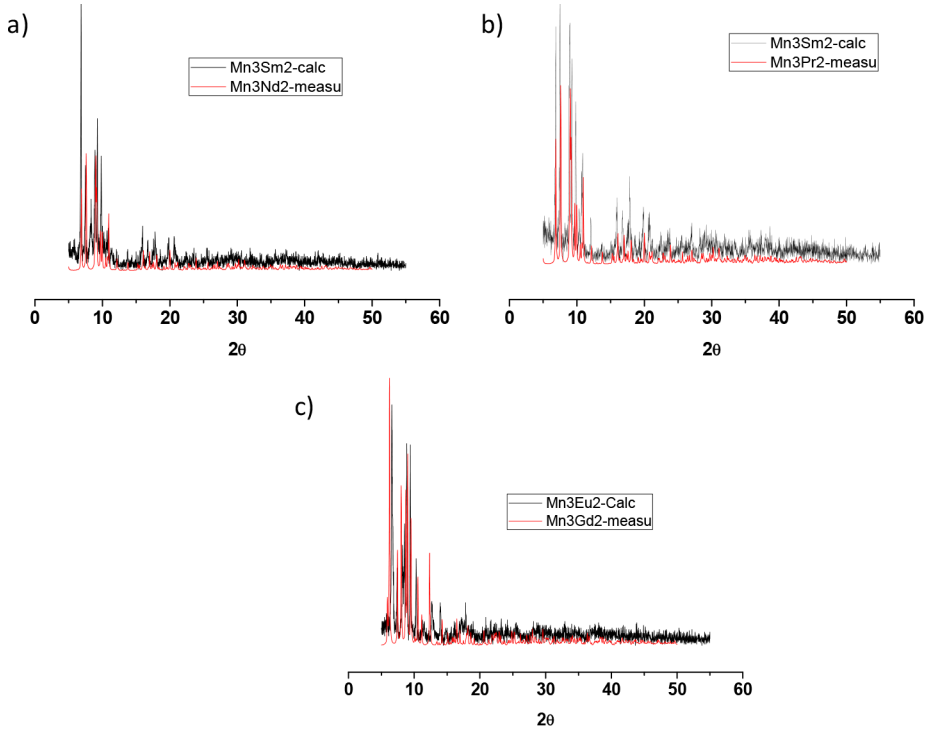

Figure 2. X-ray powder diffraction patterns measured for complexes (a) **6-Nd**, (b) **7-Pr**, and (c) **8-Gd**.

DOI: 10.1021/acs.inorgchem.7b02608
Inorg. Chem. 2018, 57, 1158−1170

The molecular structures of **1-Dy** to **7-Pr** (benz) and **8-Gd** and **9-Eu** (*o*-tol) are essentially identical, the only difference being the replacement of the benzoate ligand with *o*-toluate. Therefore, only complex **1** is described in detail and is representative of all complexes. Compound **1-Dy** is a heterometallic pentanuclear $\{Mn^{IV}Mn^{III}_2Dy^{III}_2\}$ complex (Figure 1) that consists of one Mn^{IV}, two Mn^{III}, and two Dy^{III} ions. The oxidation state of the ions was determined via charge balance, structural considerations, and bond valence sum calculations (see Table S2 in the Supporting Information). The metallic core displays a distorted trigonal bipyramidal motif (see Figure 1, bottom right). On the other hand, the structure also resembles an arrangement like that found for the $\{TM^{III}_2Ln^{III}_2\}$ (TM = Co, Cr) butterfly complexes.[16a,c,17,46] In those cases, all four ions lie in a plane, with the Ln^{III} ions in the body (central) positions and the TM ions in the wing (outer) sites. For **1-Dy** we observe half of the butterfly motif (Dy1, Dy2, and Mn3, with the same ligand bridging arrangement); however, we then find two manganese ions lying above and below these three ions instead of the usual one (Figure 1, top right). The ions in the complex are held together by bridging $[mdea]^{2-}$, $[O^{2-}]$, and benzoate ions and chelating and terminal $[NO_3]^-$ and MeOH ions/ligands. The Dy^{III} ions are nine-coordinate with capped-square-antiprismatic geometries with an $\{DyO_9\}$ coordination sphere. The Mn^{IV} center displays a $\{MnNO_5\}$ coordination sphere with an octahedral geometry, while the two other Mn^{III} centers are in a $\{MnNO_4\}$ coordination sphere with distorted-square-pyramidal geometries. Selected bond lengths and bond angles are given in Table S3 in the Supporting Information.

Magnetic Properties of the $\{Mn^{IV}Mn^{III}_2Ln^{III}_2\}$ Pentanuclear Complexes. *Direct Current Magnetic Susceptibility Measurements.* The variations with temperature of the direct current (dc) magnetic susceptibilities of all complexes are shown in Figure 3. The magnetic data are summarized in Table 1. The complexes are split into three groups for comparison. The first group depicts the benzoate family with **1-Dy**, **2-Tb**, and **3-Gd** complexes. The **2-Tb** and **3-Gd** complexes display a gradual decrease in the $\chi_M T$ product as the temperature is reduced, before an increase is noted at low temperatures. At the lowest temperatures, the $\chi_M T$ value reaches a maximum before decreasing again. This would indicate that both complexes display some form of ferromagnetic interactions (Figure 3, top and bottom). Complex **1-Dy**, on the other hand, reveals a continual decrease in the $\chi_M T$ product, with an abrupt decrease below ~10 K, suggestive of Zeeman level depopulation effects and the likelihood of dominant intramolecular antiferromagnetic interactions (Figure 3, top).

The second group depicts the benzoate family with complexes **4-Eu**, **5-Sm**, **6-Nd**, and **7-Pr**. In all cases a steep decrease in $\chi_M T$ is observed over the entire temperature range (Figure 3, middle), again indicating Zeeman level depopulation effects and the likelihood of dominant intramolecular antiferromagnetic interactions. The *o*-toluate series **8-Gd** and **9-Eu** also revealed a continual decrease in the $\chi_M T$ product occurring below room temperature, which is indicative of antiferromagnetic interactions (Figure 3). It is interesting to note that the molecular structures of compounds **3-Gd** and **8-Gd** are identical except for the difference in the carboxylate ligand used but display significantly different $\chi_M T$ versus T profiles.

Isothermal M versus H plots for all complexes are shown in Figures S1 and S2 in the Supporting Information. The plots show gradual increases with increasing H, at low fields and low temperatures, with M then increasing linearly at larger fields, without coming close to a saturation value, indicating anisotropy and/or antiferromagnetic interactions. The best fits of the M/H plots are also given.

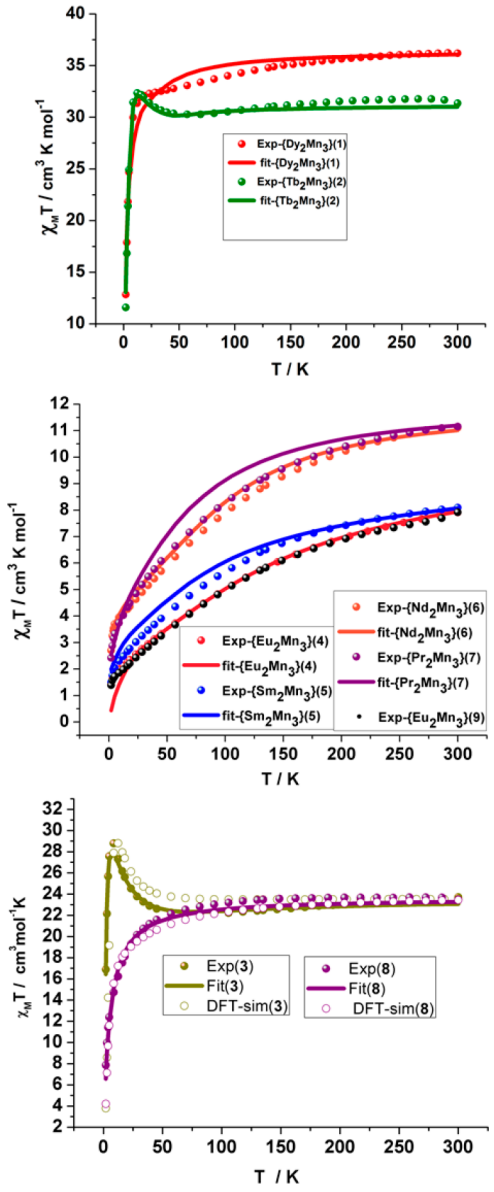

Figure 3. Measured and POLY_ANISO-fitted magnetic susceptibilities of **1-Dy** and **2-Tb** (top); **4-Eu** to **7-Pr** and **9-Eu** (middle); and **3-Gd** and **8-Gd** (bottom) from 300 to 2 K under a magnetic field of 1 T. The PHI-fitted and DFT-simulated plots are shown as solid lines and open circles; see inset.

To elucidate the magnetic exchange interactions for **3-Gd** and **8-Gd**, fits were attempted using the PHI program[36] employing the isotropic four J Hamiltonian shown in Figure 4 and eq 1. Best fit parameters are $J_1 = 0.13$ cm^{-1}, $J_2 = 0.27$ cm^{-1}, $J_3 = -0.23$ cm^{-1}, and $J_4 = -2.90$ cm^{-1} for **3-Gd** and $J_1 = -0.08$ cm^{-1}, $J_2 = 0.03$ cm^{-1}, $J_3 = -0.54$ cm^{-1}, and $J_4 = -1.03$ cm^{-1} for **8-Gd** (Figure 3, bottom, solid lines). The values obtained from the fit for Gd(III)−Gd(III) (J_1) and Mn(III)−Gd(III) (J_3) interactions are in good agreement with the previously reported values for these interactions.[47] The Mn(IV)−Gd(III) (J_2) interaction has no precedence but lies in the range of values expected for 3d-Gd interactions[47c,48] that offers confidence in the obtained J parameters.

DOI: 10.1021/acs.inorgchem.7b02608
Inorg. Chem. 2018, 57, 1158−1170

Table 1. dc Magnetic Data Recorded for All Pentanuclear Compounds

complex	ground state			Curie constant expected for the complex (cm^3 K mol^{-1})	obsd $\chi_M T$ (cm^3 K mol^{-1})		obsd M ($N\mu_B$) at 2 K and 5 T
	Ln^{III} ion	Mn^{IV} ion	Mn^{III} ion		300 K	2 K	
1-Dy	Dy^{III}; $^6H_{15/2}$ (g = 4/3)	S = 3/2 (g = 2)	S = 2 (g = 2)	36.2	36.2	30.3	14.0
2-Tb	Tb^{III}; $^7F_6$ (g = 3/2)	S = 3/2 (g = 2)	S = 2 (g = 2)	31.6	31.3	39.3	13.8
3-Gd	Gd^{III}; $^8S_{7/2}$ (g = 2)	S = 3/2 (g = 2)	S = 2 (g = 2)	23.7	23.7	38.0	18.8
4-Eu	Eu^{III}; $^7F_0$ (g = 0)	S = 3/2 (g = 2)	S = 2 (g = 2)	7.9	7.9	1.4	2.7
5-Sm	Sm^{III}; $^6H_{5/2}$ (g = 2/7)	S = 3/2 (g = 2)	S = 2 (g = 2)	8.1	8.1	1.5	3.2
6-Nd	Nd^{III}; $^4I_{9/2}$ (g = 8/11)	S = 3/2 (g = 2)	S = 2 (g = 2)	11.1	11.1	2.7	5.6
7-Pr	Pr^{III}; $^3H_4$ (g = 4/5)	S = 3/2 (g = 2)	S = 2 (g = 2)	11.1	11.1	2.4	4.3
8-Gd	Gd^{III}; $^8S_{7/2}$ (g = 2)	S = 3/2 (g = 2)	S = 2 (g = 2)	23.7	23.5	7.9	10.4
9-Eu	Eu^{III}; $^7F_0$ (g = 0)	S = 3/2 (g = 2)	S = 2 (g = 2)	7.9	7.9	1.4	2.6

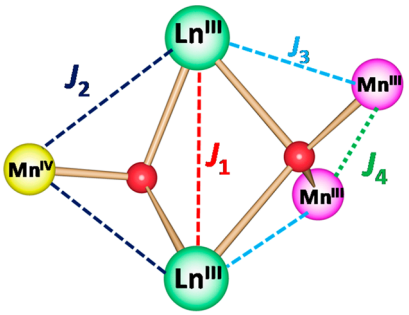

Figure 4. Magnetic exchange interactions in **1-Dy** to **8-Gd**.

Alternating Current Magnetic Susceptibility Measurements. The magnetization dynamics were investigated for each complex by alternating current (ac) susceptibility measurements as a function of both temperature and frequency. A 3.5 Oe ac field was employed, with a zero-static dc field for **1-Dy** and **7-Pr** (see Figure 5); dc fields of 2000 and 3000 Oe were necessary for **2-Tb**, **4-Eu**, **8-Gd**, and **9-Eu**. A nonzero out-of-phase (χ_M'') component is observed for **1-Dy** and **7-Pr**; however, no maxima are observed with H_{dc} = 0 Oe (Figure 5). This does not prove SMM behavior but suggests the possibility of such behavior, with a small energy barrier in the magnetic reorientation. No out-of-phase signals are observed at temperatures below 1.8 K for **2-Tb** to **6-Nd**, **8-Gd**, and **9-Eu** under H_{dc} = 0 Oe. Out-of-phase susceptibility signals are, however, observed for complexes **2-Tb**, **4-Eu**, **8-Gd**, and **9-Eu**, in the presence of a static dc field (2000 and 3000 Oe) (Figure S3 in the Supporting Information). Complexes **4-Eu** and **9-Eu** contain paramagnetic Mn^{III}/Mn^{IV} and diamagnetic Eu^{III} ions only: therefore, the slow magnetic relaxation must be a consequence of the Mn^{IV}/Mn^{III} ions. No SMM behavior was observed above 1.8 K for **3-Gd**, **5-Sm**, and **6-Nd** in view of the absence of any frequency-dependent out-of-phase (χ_M'') signals in both zero and applied dc fields (see Figure S4 in the Supporting Information).

Estimation of Exchange Coupling in Complexes 3-Gd and 8-Gd Using DFT Calculations. DFT calculations were performed on complexes **3-Gd** and **8-Gd** to obtain exchange parameters for pairwise Gd^{III}–Gd^{III} (J_1), Mn^{IV}–Gd^{III} (J_2), Mn^{III}–Gd^{III} (J_3), and Mn^{III}–Mn^{III} (J_4) interactions using their X-ray crystal structures as input (see Computational Details for methodology employed and Figure 5 for the exchange topology). The calculations yield values of J_1 = 0.07 cm^{-1}, J_2 = 1.21 cm^{-1}, J_3 = −0.45 cm^{-1}, and J_4 = −3.77 cm^{-1} for **3-Gd**. The signs of the computed J values agree with those obtained from the fit of the experimental susceptibility data; however, from the DFT calculations the magnitude is slightly smaller for J_1, and slightly larger for J_2, J_3, and J_4. Although J_1 is very weakly ferromagnetic, the overall ferromagnetic nature of the magnetic susceptibility curve (Figure 3, bottom) is reproduced with inclusion of a small intermolecular interaction (zJ = 0.01 cm^{-1}). DFT calculations yield exchange interactions of J_1 = −0.07 cm^{-1}, J_2 = 1.20 cm^{-1}, J_3 = −0.45 cm^{-1}, and J_4 = −3.34 cm^{-1} for **8-Gd**. These J values also reproduce the sign of the experimental exchange constants, but the magnitude is slightly larger for J_2

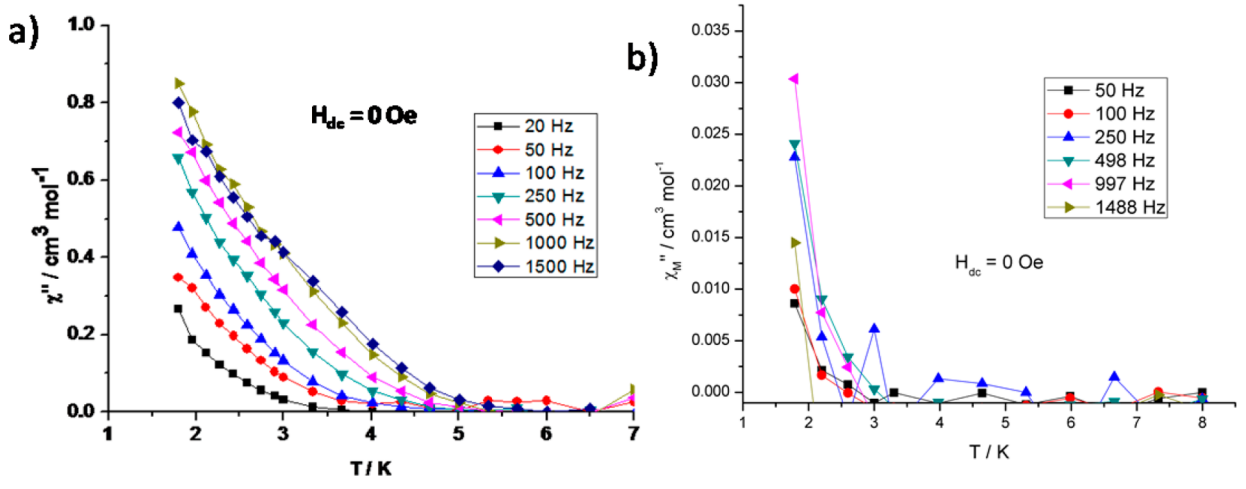

Figure 5. Plot of χ_M'' versus T at the frequencies indicated for (a) **1-Dy** and (b) **7-Pr** under H_{dc} = 0 Oe.

DOI: 10.1021/acs.inorgchem.7b02608
Inorg. Chem. 2018, 57, 1158–1170

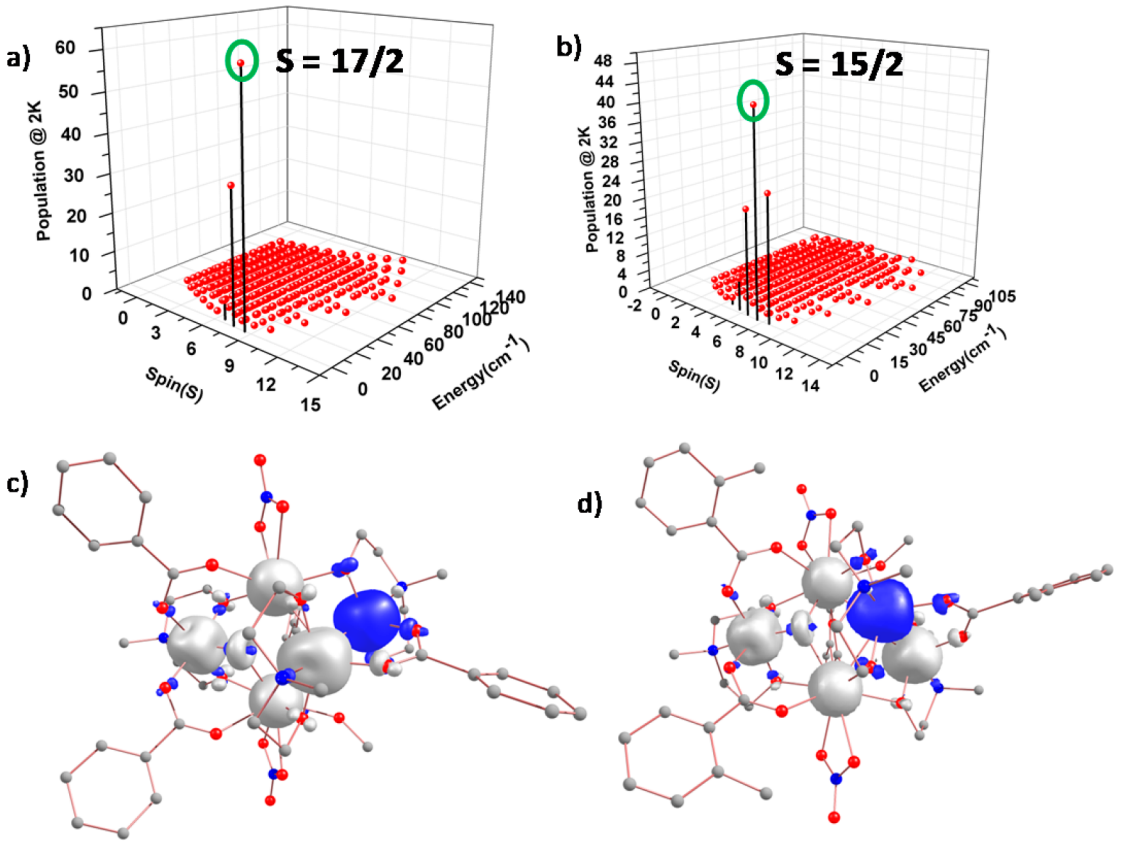

Figure 6. Computed energy levels showing low-lying magnetic states for (a) complex **3-Gd** and (b) complex **8-Gd**. The ground state is highlighted in green circles with the values of {**3-Gd**, S = 17/2} and {**8-Gd**, S = 15/2}. DFT-computed high-spin density plots of (c) complex **3-Gd** and (d) complex **8-Gd**. The white and blue colors represent positive and negative spin densities, respectively.

and J_4 in comparison to the experimental data fit. In our analysis we have assumed that the structural parameters derived from the X-ray data of Eu (**9-Eu**) will be very similar to that of Gd (**8-Gd**); however, it is possible that some geometrical parameters are different, leading to the difference in the observed behavior. Although complexes **3-Gd** and **8-Gd** are similar, we find, however, a significant difference in the low-temperature susceptibility behavior (Figure 3, bottom). We find that the change of ligand, surprisingly, causes the intracluster coupling in these two complexes to change from net ferromagnetic (**3-Gd**) to antiferromagnetic (**8-Gd**), leading to a change in the nature of the ground state and thus the temperature-dependent susceptibility profile. We note that the set of DFT J parameters reproduces the susceptibility data very well (Figure 3, bottom).

To rationalize the origin of the ferromagnetic Gd^{III}–Gd^{III} exchange in **3-Gd** and antiferromagnetic exchange in **8-Gd**, overlap integrals for the Gd^{III}–Gd^{III} pair have been computed. For complex **8-Gd**, 20 seven dominant 4f–4f overlaps are noted in 49 possible overlaps, while in complex **3-Gd** only 9 4f-4f overlaps are noted, with such interactions leading to a net antiferromagnetic interaction in the former and ferromagnetic interaction in the latter case (see Tables S4 and S5 in the Supporting Information).[49] Small variations in the structural parameters such as Gd–O–Gd and Gd–O–Gd–O dihedral angles are responsible for the observed differences (see Table S3 in the Supporting Information). With fixed Gd–Gd exchange we have not obtained any good susceptibility fit (see Figure S5 in the Supporting Information). It explains the importance of Gd–Gd exchange in complexes **3-Gd** and **8-Gd**.

For **3-Gd** and **8-Gd**, the DFT-computed J values yielded S = 17/2 and S = 15/2 as the ground states, respectively (see Figure 6a,b). This is in line with the experimental magnetization saturation (or near saturation) value of ∼17 Nμ_B for **3-Gd**, but the value was overestimated for **8-Gd** (Figure S2b in the Supporting Information). In **3-Gd**, the dominant interaction is an antiferromagnetic J_4 interaction, which leads to a spin-down configuration in one of the Mn^{III} ions, and the second dominant interaction being J_2 (ferromagnetic) leads to a spin-up configuration for Mn^{IV} and Gd^{III} ions. This leads to an S = 17/2 ground state spin configuration, as shown in Figure 6c. For complex **8-Gd** a similar kind of situation is expected; however, competing exchange interactions within the structure leads to an S = 15/2 ground state (see Figure 6d).

Mechanism of Magnetization Blockade. We have performed ab initio CASSCF calculations on **1-Dy**, **2-Tb**, **5-Sm**, **6-Nd**, and **7-Pr** using MOLCAS 8.0 (see Computational Details) to interpret the anisotropy of the Ln^{III} and the Mn^{III}/Mn^{IV} ions. CASSCF calculations reveal D values of −2.9 and −3.0 cm^{-1} for the Mn^{III} ions (Mn2 and Mn3, respectively), with a small E/D ratio. These values are in line with those expected for Mn^{III} ions.[50] The D value of the Mn^{IV} ion is computed to be +0.5 cm^{-1}. To fully comprehend the observed relaxation mechanism of these molecules, two sets of calculations were performed. First, we performed calculations on a mononuclear Ln^{III} fragment to analyze and understand the magnetic relaxation that originates from the single ion, and second, we performed an analysis of the exchange-coupled $\{Mn^{IV}Mn_2^{III}Ln_2^{III}\}$ system

DOI: 10.1021/acs.inorgchem.7b02608
Inorg. Chem. 2018, 57, 1158–1170

incorporating the computed anisotropy of the Mn and Ln ions and the exchange coupling. The single-ion analysis will be discussed first followed by the exchange-coupled scenario. Moreover, we find that the anisotropy of the Mn^{III} ions alone offers the possibility of SMM behavior in **4**, **8**, and **9** (where the Ln ions do not contribute to the anisotropy) under applied field conditions. A plausible relaxation mechanism developed using only the exchange coupled states of the Mn ions for complexes **4-Eu**, **8-Gd**, and **9-Eu** is shown in Figure S6 in the Supporting Information. Though the individual single-ion anisotropy of the Mn^{III} ions is certainly large, these axes are noncollinear and thus likely to reduce the overall anisotropy of the complex. This is reflected in the relaxation mechanism developed where a negligible energy barrier of 0.13 cm^{-1} has been computed, and this is in line with the experimental observations.

Dynamics of Magnetization from Single-Ion Anisotropy of Ln^{III} Ions. We begin our discussion with molecules possessing Kramers ions (complexes **1-Dy**, **5-Sm**, and **6-Nd**) and later expand this to complexes containing non-Kramers ions (complexes **2-Tb** and **7-Pr**).

The g values for each Ln^{III} site in the ground Kramers doublet (KD) of **1-Dy**, **5-Sm**, and **6-Nd** are calculated and shown in Table 2 and Table S7 in the Supporting Information.

Table 2. Low-Lying Energies (cm^{-1}) and g Tensors of Ln Fragments That Originate from the Corresponding Ground Kramers Doublet in 1-Dy, 5-Sm, and 6-Nd

	1-Dy		5-Sm		6-Nd	
	Dy1	Dy2	Sm1	Sm2	Nd1	Nd2
	0.0	0.0	0.0	0.0	0.0	0.0
	20.5	52.3	130.2	79.9	143.8	103.8
	67.3	103.8	292.8	212.8	201.6	169.8
	122.2	153.8	1080.4	1064.9	311.9	289.7
	197.0	226.8	1197.5	1147.7	412.1	367.7
	278.1	303.0	1277.9	1224.9	2064.0	2059.2
	351.0	359.2	1375.6	1306.6	2133.9	2115.8
	419.6	453.7	2353.6	2347.0	2170.1	2135.6
g_x	0.0092	0.0640	0.1220	0.1642	0.8975	1.3640
g_y	0.4340	0.6179	0.2164	0.3226	1.8436	2.1029
g_z	18.7250	18.4073	1.0928	1.1165	4.3910	3.9623

The computed g_{zz} orientation for the ground-state KD in **1-Dy** is shown in Figure 7a and the same is observed for **5-Sm**, and **6-Nd**. The g values explain the splitting of the two components of the Kramers doublet in a magnetic field for **1-Dy**, **5-Sm**, and **6-Nd**. For both Ln^{III} ions, a significant transverse anisotropy is detected in each complex with the transverse component for Ln1 < Ln2 (see Table 2). This suggests that the two Ln^{III} ions in each complex are in different environments. The angle between the two g_{zz} axes of Ln^{III} ions is tilted by 40.8° for **1-Dy**, 116.3° for **5-Sm**, and 112.9° for **6-Nd**. The large transverse components (g_x and g_y) of Kramers ions (Dy, Sm, and Nd) suggests that the blockage of magnetization at individual Ln ions could not be achieved due to fast QTM. The qualitative mechanisms for the magnetic relaxation at each Ln site (Ln1 and Ln2) of **1-Dy**, **5-Sm**, and **6-Nd** are shown in Figure 8. The transverse components are very large in **5-Sm** and **6-Nd** in comparison to **1-Dy**, which suggests that the single-ion anisotropy of the Ln^{III} ions in **5** and **6** is unlikely to help magnetization blockade, leading to an absence of SMM behavior for these two molecules. The first excited Kramers doublet (state ±2) lies above the ground state KDs with an energy gap of 20.5 and 52.3 cm^{-1} for Dy1 and Dy2, respectively, in **1-Dy**, 130.2 and 79.9 cm^{-1} for Sm1 and Sm2, respectively, in **5-Sm**, and 143.8 and 103.7 cm^{-1} for Nd1 and Nd2, respectively, in **6-Nd**. In all three cases, the first excited KD also possesses a large transverse anisotropy (see Table 2 and Table S5 in the Supporting Information). The first excited states for Nd^{III} are found to be the largest among the three complexes; however, the ground state wave functions are strongly mixed, leading to significant tunneling, and this cannot possibly be quenched by an applied dc field or weak exchange coupling interactions.

The g values for each Ln^{III} site in the ground Ising doublets of **2-Tb** and **7-Pr** are calculated and shown in Table 3 and Table S8 in the Supporting Information. The computed g_{zz} orientations for the ground-state KD in **2-Tb** is shown in Figure 7b and the same is observed for **7-Pr**. The angle between the two g_{zz} axis of the Ln^{III} ions is tilted by 2.74° for **2-Tb** and 21.41° for **7-Pr**. In **2-Tb** and **7-Pr**, the **g** tensor of the ground Ising doublet of individual Ln centers is axial with the zero transverse components (g_x and g_y); however, the Ln ions are in different environments. The tunneling gaps (Δ_{tun}) between the ground state Ising doublets are large: 8.9×10^{-2} and 0.182 cm^{-1} for Tb1 and Tb2, respectively, in **2-Tb** and 46.2 and 34.1 cm^{-1} for Pr1 and Pr2, respectively, in **7-Pr** (see Table 3 and Table S6 in the Supporting Information). Therefore, from a single-ion perspective this leads to relaxation of magnetization through the ground state in **2-Tb** and **7-Pr** and suggests that single-ion anisotropy blockade is not possible in the presence and absence of a dc field.

The crystal field (CF, B_k^q) parameters for complexes **1-Dy**, **5-Sm**, and **6-Nd** are analyzed for deeper insight into the mechanism of magnetic relaxation. The corresponding crystal field Hamiltonian is given by

$$\hat{H}_{CF} = \sum \sum_{k=-q}^{q} B_k^q \tilde{O}_k^q \quad (3)$$

where B_k^q is the crystal field parameter, while O_k^q is the Stevens operator.

The QTM probability of ground state KDs is explained by the parameters. The CF parameters for complexes **1-Dy**, **5-Sm**, and **6-Nd** are given in Table S10 in the Supporting Information. The QTM processes are dominant when the nonaxial (in which $q \neq 0$ and $k = 2, 4, 6$) terms are larger than the axial terms (in which $q = 0$ and $k = 2, 4, 6$). In these complexes, nonaxial terms are larger than axial terms, leading to a larger transverse anisotropy term and fast QTM relaxation, and this has been proved experimentally as well.[51]

Dynamics of Magnetization from the Exchange-Coupled {Mn_3Ln_2} System (Ln = Dy, Tb, Sm, Nd, Pr). Using the POLY_ANISO program,[43] the exchange interactions between anisotropic lanthanide magnetic centers (Ln^{III}–Ln^{III}, J_1), two Mn^{IV}–Ln^{III} (J_2), two Mn^{III}–Ln^{III} (J_3), and Mn^{III}–Mn^{III} (J_4) interactions were simulated within the Lines model.[44] The simulated magnetic exchange interactions of **1-Dy**, **2-Tb**, **5-Sm**, **6-Nd**, and **7-Pr** are shown in Table 4. The exchange interactions between magnetic ions were calculated on the basis of the lowest states that were obtained from the ab initio calculations for magnetic sites of both Ln^{III} ions and the three Mn^{III} ions.

All of the exchange interactions (J_1–J_4) of **1-Dy**, **5-Sm**, **6-Nd**, and **7-Pr** are found to be antiferromagnetic, while in **2-Tb**, the J_1 and J_2 interactions are found to be ferromagnetic in nature.

DOI: 10.1021/acs.inorgchem.7b02608
Inorg. Chem. 2018, 57, 1158–1170

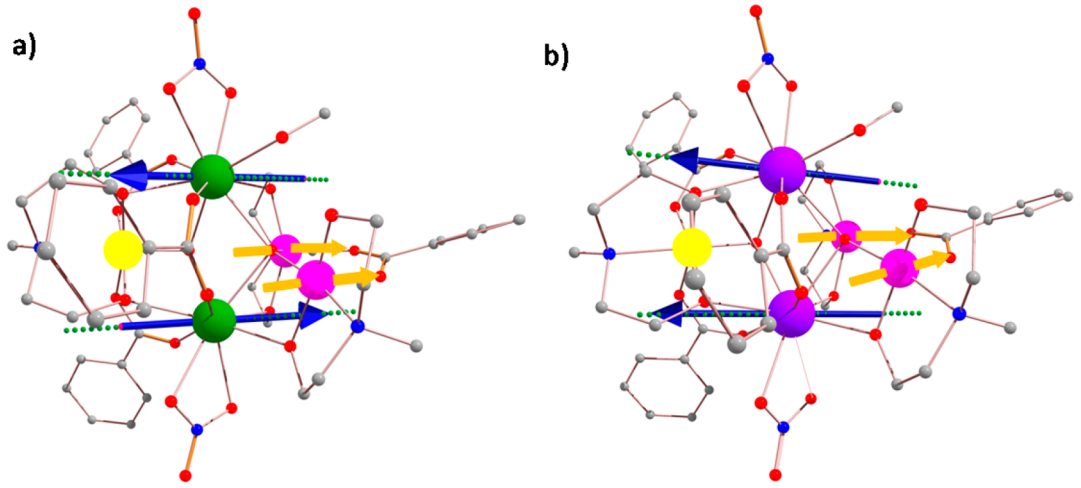

Figure 7. Orientations of the local magnetic moments in the ground doublet of complexes (a) **1-Dy** and (b) **2-Tb**. The blue arrows show the antiferromagnetic coupling in **1-Dy** and ferromagnetic coupling in **2-Tb** of the local magnetic moments of the Ln ions in the ground state. The yellow arrows are the D_{zz} direction of Mn^{III} ions.

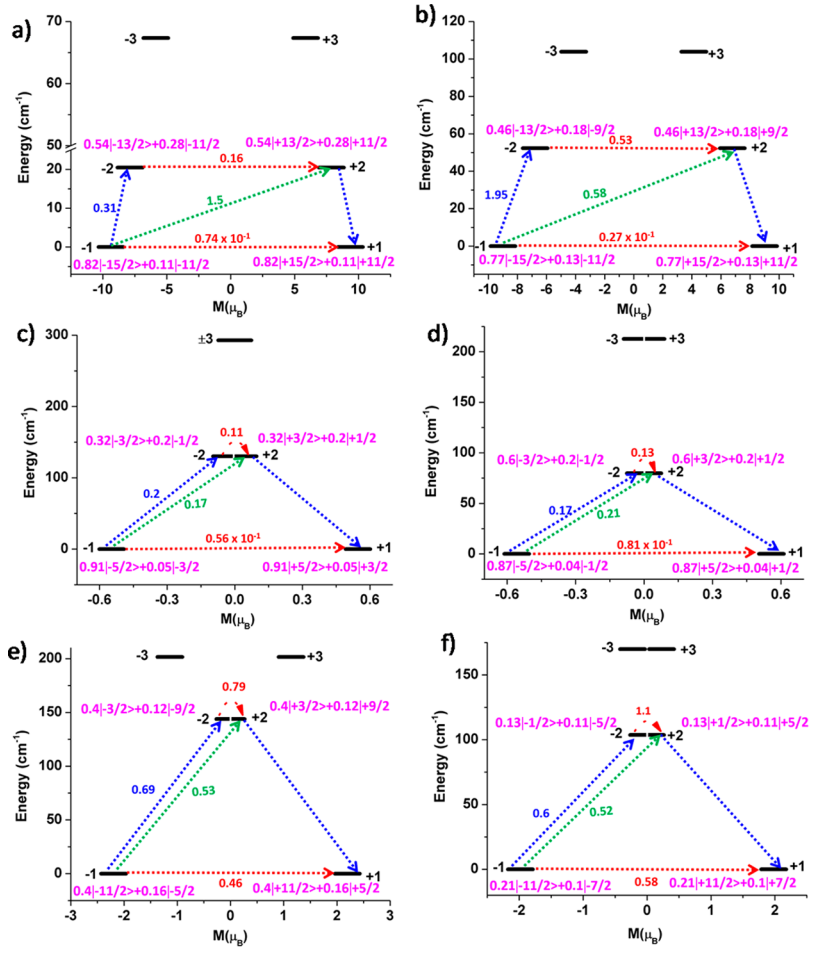

Figure 8. Ab initio computed magnetization blocking barrier for (a) the Dy1 site in **1-Dy**, (b) the Dy2 site in **1-Dy**, (c) the Sm1 site in **5-Sm**, (d) the Sm2 site in **5-Sm**, (e) the Nd1 site in **6-Nd**, and (f) the Nd2 site in **6-Nd**. The thick black line indicates the KDs as a function of the computed magnetic moment. The green/blue arrows show the possible pathway through the Orbach/Raman relaxation. The dotted red lines represent the presence of QTM and thermally activated quantum tunneling of magnetization (TA-QTM) between the connecting pairs. The numbers provided at each arrow are the mean absolute values for the corresponding matrix element of the transition magnetic moment.

The calculations reproduce the magnetic susceptibility and magnetization of **1-Dy**, **2-Tb**, **5-Sm**, **6-Nd**, and **7-Pr** well (see Figure 3, top and middle, and Figure S1 in the Supporting Information) with the inclusion of a small intermolecular interaction (zJ). To reproduce the magnetic susceptibility of **4-Eu** (see Figure 3, middle), only the lowest states of Mn^{IV} and two Mn^{III} ions were considered. Due to the diamagnetic nature of Eu^{III} ions ($^7F_0$) only the Mn^{III}–Mn^{III} (J_4) exchange is

DOI: 10.1021/acs.inorgchem.7b02608
Inorg. Chem. 2018, 57, 1158−1170

Table 3. Low-Lying Energies (cm^{-1}) and g Tensors of the Ln^{III} Fragments That Originate from the Corresponding Ground Ising Doublet in 2-Tb and 7-Pr

	2-Tb		7-Pr	
	Tb1	Tb2	Pr1	Pr2
	0.0	0.0	0.0	0.0
	0.1	0.2	46.2	34.1
	117.4	93.4	71.1	81.2
	117.9	99.0	112.2	92.3
	196.3	145.4	229.2	238.8
	200.5	157.4	361.4	320.3
	253.2	175.6	401.0	341.9
	261.1	217.4	516.3	425.0
	284.0	224.2	528.2	447.7
g_x	0.0000	0.0000	0.0000	0.0000
g_y	0.0000	0.0000	0.0000	0.0000
g_z	17.7603	17.6333	4.3950	4.2573

Table 4. Magnetic Interactions (cm^{-1}) between Magnetic Ions in 1-Dy, 2-Tb, 5-Sm, 6-Nd, and 7-Pr

	POLY_ANISO fitted				
complex	J_1	J_2	J_3	J_4	zJ
1-Dy	−0.1	−0.01	−0.01	−0.2	−0.01
2-Tb	0.02	0.3	−0.35	−0.45	−0.01
5-Sm	−0.8	−0.5	−0.5	−6.3	−0.01
6-Nd	−0.5	−0.1	−0.2	−5.0	−0.01
7-Pr	−0.8	−0.8	−0.8	−5.8	−0.01

considered, which yielded a J value of −5.8 cm^{-1}. To avoid the problem of overparametrization while performing the fit using the Lines model, we have performed additional simulations where J_1 and J_4 values are kept constant with those obtained from DFT estimates for the Gd analogues. However, this yielded a very poor fit to the experimental data, and this suggests that all parameters are varying as we move from Gd to other Ln complexes (see Figure S5 and Table S11 in the Supporting Information).

In **1-Dy** and **7-Pr**, the QTM values between the ground exchange coupled state are computed to be small (see Figure 9); however, QTM becomes large at the excited states, which causes magnetic relaxation via these states with a small energy barrier (1.74 and 1.0 cm^{-1} for **1-Dy** and **7-Pr**, respectively). Further to this, the noncollinearity between the g_{zz} orientation of the Ln^{III} ions and the D_{zz} orientation of the Mn^{III} ions and the very weak Ln^{III}−Ln^{III} and $Mn^{III/IV}$−Ln^{III} interactions lead to the fast reversal of magnetization in these complexes.[52] This explains the lack of a maximum above 1.8 K in the experimental out-of-phase ac magnetic susceptibilities for **1-Dy** and **7-Pr** (H_{dc} = 0 Oe). We note that this is the first example of a complex containing a Pr^{III} ion to display SMM behavior in the absence of an applied static magnetic field. For complexes **2-Tb**, **5-Sm**, and **6-Nd**, the QTM probability between the ground and first exchange coupled state is large. Thus, magnetic relaxation occurs through the ground state with a negligible energy barrier (see Figure S7 in the Supporting Information). We therefore predict from our calculations that compounds **2-Tb**, **5-Sm**, and **6-Nd** do not act as SMMs, which is what we find from the ac experiment with H_{dc} = 0 Oe.

We have attempted to utilize Mn−Ln exchange to quench the QTM effects and enhance the barrier height for magnetization reversal. Although Mn^{III} ions are ideally suited for this purpose as they possess significant anisotropy, the nature of the Mn^{III}−Ln^{III} and Mn^{IV}−Ln^{III} exchange is found to be weak in all of the examples studied. This is essentially due to the weak mixing of the 3d orbitals of the Mn ions with the lanthanide 4f orbitals. Significant overlap can be expected for the σ-type d_{z^2} orbital of the Mn^{III} ions and the Ln^{III} 4f orbitals; however, the orientation of the d_{z^2} orbital of the Mn^{III} ion is not favorable for overlap in these examples as it does not lie along the axis of the bridging ligands connecting the Mn^{III} and Ln^{III} ions (see Figure 1). This renders the Mn^{III}−Ln^{III} exchange very weak and can quench only the weak/moderate QTM effects observed. In addition, the anisotropic axes of the Mn ions are not collinear with the g_{zz} axis of the Ln^{III} ions, triggering faster relaxation and very small barrier height for magnetization reversal.

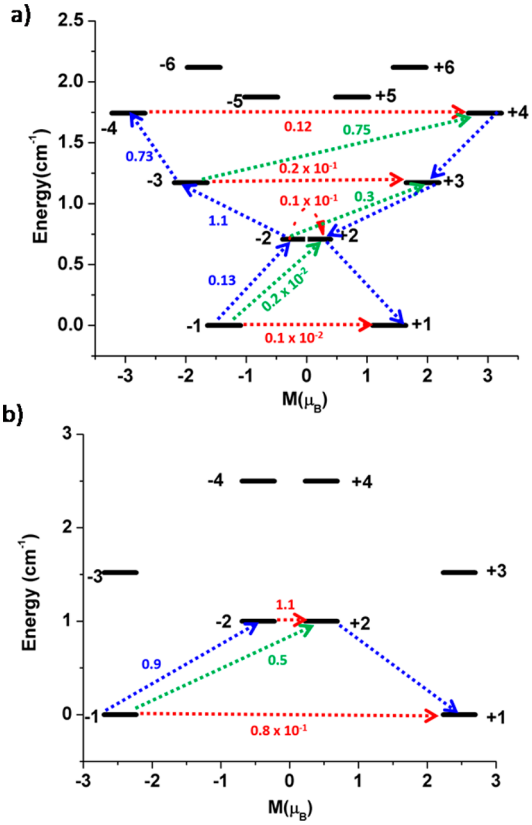

Figure 9. Low-lying exchange spectra in (a) **1-Dy** and (b) **7-Pr**. The exchange states are placed on the diagram according to their magnetic moments (bold black lines). The dotted red lines represent the presence of QTM/TA-QTM between the connecting pairs, and the green/blue arrows show the possible pathway through the Orbach/Raman relaxation. The numbers at the paths are averaged transition moments in μ_B, connecting the corresponding states.

CONCLUSIONS

We have presented a new family of pentanuclear $\{Mn^{III}_2Mn^{IV}Ln^{III}_2\}$ coordination complexes (Ln = Dy, Tb, Gd, Sm, Nd, and Pr) with a distorted-trigonal-bipyramidal metal topology that is obtained by use of a multiligand reaction approach. From the magnetic susceptibility data ($\chi_M T$ vs T) all complexes display net antiferromagnetic coupling, except for **2-Tb** and **3-Gd**, which show net ferromagnetic coupling. Interestingly, complexes **3-Gd** and **8-Gd** which display the same metal ion arrangement, $\{Mn^{III}_2Mn^{IV}Gd^{III}_2\}$, and differ only in the nature of the carboxylate ligand coordinated; benzoate (**3-Gd**) and *o*-toluate

DOI: 10.1021/acs.inorgchem.7b02608
Inorg. Chem. 2018, 57, 1158−1170

(**8-Gd**) reveal a significant difference in the $\chi_M T$ vs T profile. Fits of the experimental data and a DFT analysis reveal that the difference stems from the nature of the Gd^{III}–Gd^{III} exchange interaction, which switches from ferromagnetic in **3-Gd** to antiferromagnetic in **8-Gd**. This is due to different Gd–O–Gd angles and Gd–O–Gd–O dihedral angles between **3-Gd** and **8-Gd**.

Complexes **1-Dy** and **7-Pr** show frequency-dependent out-of-phase signals indicative of SMM behavior (H_{dc} = 0 Oe). We also observe SMM behavior under applied static dc fields of 2000 and 3000 Oe for **2-Tb**, **4-Eu**, **8-Gd**, and **9-Eu**. Ab initio calculations predict that the origin of the zero-field SMM behavior in **1-Dy** and **7-Pr** and the applied field SMM behavior in **2-Tb** is not solely a consequence of single-ion anisotropies. Using the POLY_ANISO program, we find that the SMM behavior is attributed to very weak $Mn^{III/IV}$–Ln^{III} and Ln^{III}–Ln^{III} couplings and unfavorable $Ln^{III}/Mn^{III/IV}$ anisotropy. In addition to the ground-state QTM, the TA-QTM/Orbach/Raman process also causes the magnetic relaxation of magnetization at coupled excited states which lie just a few wavenumbers above the ground state, resulting in a very small energy barrier. In complexes **4-Eu**, **8-Gd**, and **9-Eu**, the anisotropy of Mn^{III} ions solely causes the SMM behavior under an applied field static field. We predict that the synthesis and analysis of other transition-metal-based $\{TM_3Ln_2\}$ (for e.g. TM = Cr, Fe, Co) complexes with modified structural parameters will help to unravel this relationship further and to improve SMM characteristics in the future.

■ ASSOCIATED CONTENT

Supporting Information

The Supporting Information is available free of charge on the ACS Publications website at DOI: 10.1021/acs.inorgchem.7b02608.

(PDF)

Accession Codes

CCDC 1571429–1571434 contain the supplementary crystallographic data for this paper. These data can be obtained free of charge via www.ccdc.cam.ac.uk/data_request/cif, or by emailing data_request@ccdc.cam.ac.uk, or by contacting The Cambridge Crystallographic Data Centre, 12 Union Road, Cambridge CB2 1EZ, UK; fax: +44 1223 336033.

■ AUTHOR INFORMATION

Corresponding Authors

*E-mail for K.S.M.: keith.murray@monash.edu.

*E-mail for G.R.: rajaraman@chem.iitb.ac.in.

ORCID

Gopalan Rajaraman: 0000-0001-6133-3026

Notes

The authors declare no competing financial interest.

■ ACKNOWLEDGMENTS

G.R. acknowledges financial support from the SERB of India (EMR/2014/000247) and INSA for financial support. K.S.M. and G.R. thank the Australia-India AISRF program for support. K.R.V. is thankful to the IITB-Monash Research Academy for a Ph.D. studentship.

■ REFERENCES

(1) Sessoli, R.; Gatteschi, D.; Caneschi, A.; Novak, M. A. Magnetic Bistability in a Metal-Ion Cluster. *Nature* **1993**, *365*, 141–143.

(2) (a) Gatteschi, D.; Sessoli, R.; Villain, J. *Molecular Nanomagnets*; Oxford University Press: Oxford, U.K., 2006. (b) Gatteschi, D. Molecular Magnetism: A basis for new materials. *Adv. Mater.* **1994**, *6*, 635–645.

(3) (a) Coronado, E.; Epsetin, A. J. Molecular spintronics and quantum computing. *J. Mater. Chem.* **2009**, *19*, 1670–1671. (b) Leuenberger, M. N.; Loss, D. Quantum computing in molecular magnets. *Nature* **2001**, *410*, 789–793.

(4) Bogani, L.; Wernsdorfer, W. Molecular spintronics using single-molecule magnets. *Nat. Mater.* **2008**, *7*, 179–186.

(5) Christou, G.; Gatteschi, D.; Hendrickson, D. N.; Sessoli, R. Single-molecule magnets. *MRS Bull.* **2000**, *25*, 66–71.

(6) Ako, A. M.; Hewitt, I. J.; Mereacre, V.; Clérac, R.; Wernsdorfer, W.; Anson, C. E.; Powell, A. K. A Ferromagnetically Coupled Mn_{19} Aggregate with a Record S = 83/2 Ground Spin State. *Angew. Chem., Int. Ed.* **2006**, *45*, 4926–4929.

(7) (a) Gatteschi, D.; Sessoli, R. Quantum Tunneling of Magnetization and Related Phenomena in Molecular Materials. *Angew. Chem., Int. Ed.* **2003**, *42*, 268–297. (b) Tasiopoulos, A. J.; Vinslava, A.; Wernsdorfer, W.; Abboud, K. A.; Christou, G. Giant Single-Molecule Magnets: A $\{Mn_{84}\}$ Torus and Its Supramolecular Nanotubes. *Angew. Chem., Int. Ed.* **2004**, *43*, 2117–2121.

(8) (a) Milios, C. J.; Manoli, M.; Rajaraman, G.; Mishra, A.; Budd, L. E.; White, F.; Parsons, S.; Wernsdorfer, W.; Christou, G.; Brechin, E. K. A family of $[Mn_6]$ complexes featuring tripodal ligands. *Inorg. Chem.* **2006**, *45*, 6782–6793. (b) Milios, C. J.; Vinslava, A.; Wernsdorfer, W.; Moggach, S.; Parsons, S.; Perlepes, S. P.; Christou, G.; Brechin, E. K. A record anisotropy barrier for a single-molecule magnet. *J. Am. Chem. Soc.* **2007**, *129*, 2754–2755.

(9) (a) Murugesu, M.; Habrych, M.; Wernsdorfer, W.; Abboud, K. A.; Christou, G. Single-Molecule Magnets: A Mn_{25} Complex with a Record S = 51/2 Spin for a Molecular Species. *J. Am. Chem. Soc.* **2004**, *126*, 4766–4767. (b) Stamatatos, T. C.; Foguet-Albiol, D.; Poole, K. M.; Wernsdorfer, W.; Abboud, K. A.; O'Brien, T. A.; Christou, G. Spin Maximization from S = 11 to S = 16 in Mn_7 Disk-Like Clusters: Spin Frustration Effects and Their Computational Rationalization. *Inorg. Chem.* **2009**, *48*, 9831–9845. (c) Vignesh, K. R.; Langley, S. K.; Murray, K. S.; Rajaraman, G. What Controls the Magnetic Exchange Interaction in Mixed- and Homo-Valent Mn_7 Disc-Like Clusters? A Theoretical Perspective. *Chem. - Eur. J.* **2015**, *21*, 2881–2892.

(10) (a) Ishikawa, N.; Sugita, M.; Ishikawa, T.; Koshihara, S.; Kaizu, Y. Lanthanide double-decker complexes functioning as magnets at the single-molecular level. *J. Am. Chem. Soc.* **2003**, *125*, 8694–8695. (b) Ishikawa, N.; Sugita, M.; Wernsdorfer, W. Quantum Tunneling of Magnetization in Lanthanide Single-Molecule Magnets: Bis(phthalocyaninato)terbium and Bis(phthalocyaninato)dysprosium Anions. *Angew. Chem., Int. Ed.* **2005**, *44*, 2931–2935. (c) Ishikawa, N.; Sugita, M.; Ishikawa, T.; Koshihara, S.; Kaizu, Y. Mononuclear lanthanide complexes with a long magnetization relaxation time at high temperatures: A new category of magnets at the single-molecular level. *J. Phys. Chem. B* **2004**, *108*, 11265–11271.

(11) Sessoli, R.; Powell, A. K. Strategies towards single molecule magnets based on lanthanide ions. *Coord. Chem. Rev.* **2009**, *253*, 2328–2341.

(12) Gupta, S. K.; Rajeshkumar, T.; Rajaraman, G.; Murugavel, R. An air-stable Dy(iii) single-ion magnet with high anisotropy barrier and blocking temperature. *Chem. Sci.* **2016**, *7*, 5181–5191.

(13) (a) Guo, F.-S.; Day, B. M.; Chen, Y.-C.; Tong, M.-L.; Mansikkamäki, A.; Layfield, R. A. A Dysprosium Metallocene Single-Molecule Magnet Functioning at the Axial Limit. *Angew. Chem., Int. Ed.* **2017**, *56*, 11445–11449. (b) Goodwin, C. A. P.; Ortu, F.; Reta, D.; Chilton, N. F.; Mills, D. P. Molecular magnetic hysteresis at 60 K in dysprosocenium. *Nature* **2017**, *548*, 439–442.

(14) (a) Rinehart, J. D.; Fang, M.; Evans, W. J.; Long, J. R. A N_2^{3-} Radical-Bridged Terbium Complex Exhibiting Magnetic Hysteresis at 14 K. *J. Am. Chem. Soc.* **2011**, *133*, 14236–14239. (b) Rinehart, J. D.; Fang, M.; Evans, W. J.; Long, J. R. Strong exchange and magnetic blocking in N_2^{3-}radical-bridged lanthanide complexes. *Nat. Chem.* **2011**, *3*, 538–542.

DOI: 10.1021/acs.inorgchem.7b02608
Inorg. Chem. 2018, 57, 1158–1170

(15) (a) Rajeshkumar, T.; Rajaraman, G. Is a radical bridge a route to strong exchange interactions in lanthanide complexes? A computational examination. *Chem. Commun.* **2012**, *48*, 7856−7858. (b) Singh, M. K.; Yadav, N.; Rajaraman, G. Record high magnetic exchange and magnetization blockade in $Ln_2@C_{79}N$ (Ln = Gd(iii) and Dy(iii)) molecules: a theoretical perspective. *Chem. Commun.* **2015**, *51*, 17732−17735.

(16) (a) Langley, S. K.; Chilton, N. F.; Moubaraki, B.; Murray, K. S. Anisotropy barrier enhancement via ligand substitution in tetranuclear $\{Co^{III}_2Ln^{III}_2\}$ single molecule magnets. *Chem. Commun.* **2013**, *49*, 6965−6967. (b) Vignesh, K. R.; Langley, S. K.; Murray, K. S.; Rajaraman, G. Role of Diamagnetic Ions on the Mechanism of Magnetization Relaxation in "Butterfly" $\{Co^{III}_2Ln^{III}_2\}$ (Ln = Dy, Tb, Ho). *Inorg. Chem.* **2017**, *56*, 2518−2532. (c) Langley, S. K.; Chilton, N. F.; Ungur, L.; Moubaraki, B.; Chibotaru, L. F.; Murray, K. S. Heterometallic Tetranuclear $[Ln^{III}_2Co^{III}_2]$ Complexes Including Suppression of Quantum Tunneling of Magnetization in the $[Dy^{III}_2Co^{III}_2]$ Single Molecule Magnet. *Inorg. Chem.* **2012**, *51*, 11873−11881. (d) Mishra, A.; Wernsdorfer, W.; Abboud, K. A.; Christou, G. Initial Observation of Magnetization Hysteresis and Quantum Tunneling in Mixed Manganese−Lanthanide Single-Molecule Magnets. *J. Am. Chem. Soc.* **2004**, *126*, 15648−15649. (e) Hołyńska, M.; Premužić, D.; Jeon, I.-R.; Wernsdorfer, W.; Clérac, R.; Dehnen, S. $[Mn^{III}_6O_3Ln_2]$ Single-Molecule Magnets: Increasing the Energy Barrier Above 100 K. *Chem. - Eur. J.* **2011**, *17*, 9605−9610.

(17) (a) Langley, S. K.; Wielechowski, D. P.; Vieru, V.; Chilton, N. F.; Moubaraki, B.; Abrahams, B. F.; Chibotaru, L. F.; Murray, K. S. A $\{Cr^{III}_2Dy^{III}_2\}$ Single-Molecule Magnet: Enhancing the Blocking Temperature through 3d Magnetic Exchange. *Angew. Chem., Int. Ed.* **2013**, *52*, 12014−12019. (b) Langley, S. K.; Wielechowski, D. P.; Moubaraki, B.; Murray, K. S. Enhancing the magnetic blocking temperature and magnetic coercivity of $\{Cr^{III}_2Ln^{III}_2\}$ single-molecule magnets via bridging ligand modification. *Chem. Commun.* **2016**, *52*, 10976−10979. (c) Langley, S. K.; Wielechowski, D. P.; Vieru, V.; Chilton, N. F.; Moubaraki, B.; Chibotaru, L. F.; Murray, K. S. Modulation of slow magnetic relaxation by tuning magnetic exchange in $\{Cr_2Dy_2\}$ single molecule magnets. *Chem. Sci.* **2014**, *5*, 3246−3256.

(18) Vignesh, K. R.; Langley, S. K.; Moubaraki, B.; Murray, K. S.; Rajaraman, G. Large Hexadecametallic $\{Mn^{III}−Ln^{III}\}$ Wheels: Synthesis, Structural, Magnetic, and Theoretical Characterization. *Chem. - Eur. J.* **2015**, *21*, 16364−16369.

(19) (a) Langley, S. K.; Moubaraki, B.; Forsyth, C. M.; Gass, I. A.; Murray, K. S. Structure and magnetism of new lanthanide 6-wheel compounds utilizing triethanolamine as a stabilizing ligand. *Dalton Trans.* **2010**, *39*, 1705−1708. (b) Ungur, L.; Langley, S. K.; Hooper, T. N.; Moubaraki, B.; Brechin, E. K.; Murray, K. S.; Chibotaru, L. F. Net Toroidal Magnetic Moment in the Ground State of a $\{Dy_6\}$-Triethanolamine Ring. *J. Am. Chem. Soc.* **2012**, *134*, 18554−18557.

(20) Cowieson, N. P.; Aragao, D.; Clift, M.; Ericsson, D. J.; Gee, C.; Harrop, S. J.; Mudie, N.; Panjikar, S.; Price, J. R.; Riboldi-Tunnicliffe, A.; Williamson, R.; Caradoc-Davies, T. MX1: a bending-magnet crystallography beamline serving both chemical and macromolecular crystallography communities at the Australian Synchrotron. *J. Synchrotron Radiat.* **2015**, *22*, 187−190.

(21) McPhillips, T. M.; McPhillips, S. E.; Chiu, H.-J.; Cohen, A. E.; Deacon, A. M.; Ellis, P. J.; Garman, E.; Gonzalez, A.; Sauter, N. K.; Phizackerley, R. P.; Soltis, S. M.; Kuhn, P. Blu-Ice and the Distributed Control System: software for data acquisition and instrument control at macromolecular crystallography beamlines. *J. Synchrotron Radiat.* **2002**, *9*, 401−406.

(22) Kabsch, W. Automatic processing of rotation diffraction data from crystals of initially unknown symmetry and cell constants. *J. Appl. Crystallogr.* **1993**, *26*, 795−800.

(23) Sheldrick, G. A short history of SHELX. *Acta Crystallogr., Sect. A: Found. Crystallogr.* **2008**, *64*, 112−122.

(24) Sheldrick, G. M. *SHELXL-97, Programs for X-ray Crystal Structure Refinement*; University of Göttingen, Göttingen, Germany, 1997.

(25) Barbour, L. J. *J. Supramol. Chem.* **2001**, *1*, 189−191.

(26) Noodleman, L. Valence bond description of antiferromagnetic coupling in transition metal dimers. *J. Chem. Phys.* **1981**, *74*, 5737−5743.

(27) (a) Christian, P.; Rajaraman, G.; Harrison, A.; Helliwell, M.; McDouall, J. J. W.; Raftery, J.; Winpenny, R. E. P. Synthesis and studies of a trinuclear Mn(ii) carboxylate complex. *Dalton Trans.* **2004**, 2550−2555. (b) Piligkos, S.; Rajaraman, G.; Soler, M.; Kirchner, N.; van Slageren, J.; Bircher, R.; Parsons, S.; Gudel, H.-U.; Kortus, J.; Wernsdorfer, W.; Christou, G.; Brechin, E. K. Studies of an Enneanuclear Manganese Single-Molecule Magnet. *J. Am. Chem. Soc.* **2005**, *127*, 5572−5580. (c) Rajaraman, G.; Cano, J.; Brechin, E. K.; McInnes, E. J. L. Density functional calculations of a tetradecametallic iron(iii) cluster with a very large spin ground state. *Chem. Commun.* **2004**, 1476−1477. (d) Ruiz, E.; Cano, J.; Alvarez, S.; Alemany, P. Broken symmetry approach to calculation of exchange coupling constants for homobinuclear and heterobinuclear transition metal complexes. *J. Comput. Chem.* **1999**, *20*, 1391−1400. (e) Ruiz, E.; Cano, J.; Alvarez, S.; Caneschi, A.; Gatteschi, D. Theoretical Study of the Magnetic Behavior of Hexanuclear Cu(II) and Ni(II) Polysiloxanolato Complexes. *J. Am. Chem. Soc.* **2003**, *125*, 6791−6794. (f) Ruiz, E.; Rodríguez-Fortea, A.; Cano, J.; Alvarez, S.; Alemany, P. About the calculation of exchange coupling constants in polynuclear transition metal complexes. *J. Comput. Chem.* **2003**, *24*, 982−989.

(28) (a) Berg, N.; Hooper, T. N.; Liu, J.; Beedle, C. C.; Singh, S. K.; Rajaraman, G.; Piligkos, S.; Hill, S.; Brechin, E. K.; Jones, L. F. Synthetic, structural, spectroscopic and theoretical study of a Mn(iii)-Cu(ii) dimer containing a Jahn-Teller compressed Mn ion. *Dalton Trans.* **2013**, *42*, 207−216. (b) Berg, N.; Rajeshkumar, T.; Taylor, S. M.; Brechin, E. K.; Rajaraman, G.; Jones, L. F. What Controls the Magnetic Interaction in bis-μ-Alkoxo Mn^{III} Dimers? A Combined Experimental and Theoretical Exploration. *Chem. - Eur. J.* **2012**, *18*, 5906−5918. (c) Ghosh, S.; Singh, S. K.; Tewary, S.; Rajaraman, G. Enhancing the double exchange interaction in a mixed valence $\{V^{III}$-$V^{II}\}$ pair: a theoretical perspective. *Dalton Trans.* **2013**, *42*, 16490−16493. (d) Rajaraman, G.; Murugesu, M.; Sanudo, E. C.; Soler, M.; Wernsdorfer, W.; Helliwell, M.; Muryn, C.; Raftery, J.; Teat, S. J.; Christou, G.; Brechin, E. K. A Family of Manganese Rods: Syntheses, Structures, and Magnetic Properties. *J. Am. Chem. Soc.* **2004**, *126*, 15445−15457.

(29) Singh, S. K.; Rajeshkumar, T.; Chandrasekhar, V.; Rajaraman, G. Theoretical studies on {3d-Gd} and {3d-Gd-3d} complexes: Effect of metal substitution on the effective exchange interaction. *Polyhedron* **2013**, *66*, 81−86.

(30) (a) Baker, M. L.; Timco, G. A.; Piligkos, S.; Mathieson, J. S.; Mutka, H.; Tuna, F.; Kozlowski, P.; Antkowiak, M.; Guidi, T.; Gupta, T.; Rath, H.; Woolfson, R. J.; Kamieniarz, G.; Pritchard, R. G.; Weihe, H.; Cronin, L.; Rajaraman, G.; Collison, D.; McInnes, E. J. L.; Winpenny, R. E. P. A classification of spin frustration in molecular magnets from a physical study of large odd-numbered-metal, odd electron rings. *Proc. Natl. Acad. Sci. U. S. A.* **2012**, *109*, 19113−19118. (b) Christian, P.; Rajaraman, G.; Harrison, A.; McDouall, J. J. W.; Raftery, J. T.; Winpenny, R. E. P. Structural, magnetic and DFT studies of a hydroxide-bridged $\{Cr_8\}$ wheel. *Dalton Trans.* **2004**, 1511−1512. (c) Cremades, E.; Cano, J.; Ruiz, E.; Rajaraman, G.; Milios, C. J.; Brechin, E. K. Theoretical Methods Enlighten Magnetic Properties of a Family of Mn_6 Single-Molecule Magnets. *Inorg. Chem.* **2009**, *48*, 8012−8019.

(31) Becke, A. D. Density functional thermochemistry. III. The role of exact exchange. *J. Chem. Phys.* **1993**, *98*, 5648−5652.

(32) Frisch, M. J.; Trucks, G. W.; Schlegel, H. B.; Scuseria, G. E.; Robb, M. A.; Cheeseman, J. R.; Scalmani, G.; Barone, V.; Mennucci, B.; Petersson, G. A.; Nakatsuji, H.; Caricato, M.; Li, X.; Hratchian, H. P.; Izmaylov, A. F.; Bloino, J.; Zheng, G.; Sonnenberg, J. L.; Hada, M.; Ehara, M.; Toyota, K.; Fukuda, R.; Hasegawa, J.; Ishida, M.; Nakajima, T.; Honda, Y.; Kitao, O.; Nakai, H.; Vreven, T.; Montgomery, J. A., Jr.; Ogliaro, F.; Bearpark, M.; Heyd, J. J.; Brothers, E.; Kudin, K. N.; Staroverov, V. N.; Kobayashi, R.; Normand, J.; Raghavachari, K.; Rendell, A.; Burant, J. C.; Iyengar, S. S.; Tomasi, J.; Cossi, M.; Rega, N.; Millam, J. M.; Klene, M.; Knox, J. E.; Cross, J. B.; Bakken, V.;

DOI: 10.1021/acs.inorgchem.7b02608
Inorg. Chem. 2018, 57, 1158−1170

Adamo, C.; Jaramillo, J.; Gomperts, R.; Stratmann, R. E.; Yazyev, O.; Austin, A. J.; Cammi, R.; Pomelli, C.; Ochterski, J. W.; Martin, R. L.; Morokuma, K.; Zakrzewski, V. G.; Voth, G. A.; Salvador, P.; Dannenberg, J. J.; Dapprich, S.; Daniels, A. D.; Farkas, Ö.; Foresman, J. B.; Ortiz, J. V.; Cioslowski, J.; Fox, D. J. *Gaussian 09, Revision A.02*; Gaussian, Inc., Wallingford, CT, 2009.

(33) Cundari, T. R.; Stevens, W. J. Effective core potential methods for the lanthanides. *J. Chem. Phys.* **1993**, *98*, 5555−5565.

(34) (a) Schaefer, A.; Horn, H.; Ahlrichs, R. Fully optimized contracted Gaussian basis sets for atoms Li to Kr. *J. Chem. Phys.* **1992**, *97*, 2571−2577. (b) Schaefer, A.; Huber, C.; Ahlrichs, R. Fully optimized contracted Gaussian basis sets of triple zeta valence quality for atoms Li to Kr. *J. Chem. Phys.* **1994**, *100*, 5829−5835.

(35) Bencini, A.; Totti, F. DFT description of the magnetic structure of polynuclear transition-metal clusters: The complexes $[\{Cu(bpca)_2(H_2O)_2\}\{Cu(NO_3)_2\}_2]$, (bpca = Bis(2-pyridylcarbonyl)-amine), and $[Cu(DBSQ)(C_2H_5O)]_2$, (DBSQ = 3,5-di-tert-butyl-semiquinonato). *Int. J. Quantum Chem.* **2005**, *101*, 819−825.

(36) Chilton, N. F.; Anderson, R. P.; Turner, L. D.; Soncini, A.; Murray, K. S. PHI: A powerful new program for the analysis of anisotropic monomeric and exchange-coupled polynuclear d- and f-block complexes. *J. Comput. Chem.* **2013**, *34*, 1164−1175.

(37) Aquilante, F.; Pedersen, T. B.; Veryazov, V.; Lindh, R. MOLCAS—a software for multiconfigurational quantum chemistry calculations. *WIREs Comput. Mol. Sci.* **2013**, *3*, 143−149.

(38) Hess, B. A.; Marian, C. M.; Wahlgren, U.; Gropen, O. A mean-field spin-orbit method applicable to correlated wavefunctions. *Chem. Phys. Lett.* **1996**, *251*, 365−371.

(39) Roos, B. O.; Malmqvist, P.-A. Relativistic quantum chemistry: the multiconfigurational approach. *Phys. Chem. Chem. Phys.* **2004**, *6*, 2919−2927.

(40) Roos, B. O.; Lindh, R.; Malmqvist, P.-A.; Veryazov, V.; Widmark, P.-O.; Borin, A. C. New Relativistic Atomic Natural Orbital Basis Sets for Lanthanide Atoms with Applications to the Ce Diatom and LuF_3. *J. Phys. Chem. A* **2008**, *112*, 11431−11435.

(41) Malmqvist, P. A.; Roos, B. O.; Schimmelpfennig, B. The restricted active space (RAS) state interaction approach with spin-orbit coupling. *Chem. Phys. Lett.* **2002**, *357*, 230−240.

(42) Chibotaru, L. F.; Ungur, L. Ab initio calculation of anisotropic magnetic properties of complexes. I. Unique definition of pseudospin Hamiltonians and their derivation. *J. Chem. Phys.* **2012**, *137*, 064112−22.

(43) Chibotaru, L. F.; Ungur, L. *Program POLY_ANISO*; University of Leuven, Leuven, Belgium, 2006.

(44) Lines, M. E. Orbital Angular Momentum in the Theory of Paramagnetic Clusters. *J. Chem. Phys.* **1971**, *55*, 2977−2984.

(45) (a) Neese, F. Importance of direct spin-spin coupling and spin-flip excitations for the zero-field splittings of transition metal complexes: A case study. *J. Am. Chem. Soc.* **2006**, *128*, 10213−10222. (b) Neese, F.; Petrenko, T.; Ganyushin, D.; Olbrich, G. Advanced aspects of ab initio theoretical optical spectroscopy of transition metal complexes: Multiplets, spin-orbit coupling and resonance Raman intensities. *Coord. Chem. Rev.* **2007**, *251*, 288−327.

(46) Chilton, N. F.; Langley, S. K.; Moubaraki, B.; Murray, K. S. Synthesis, structural and magnetic studies of an isostructural family of mixed 3d/4f tetranuclear 'star' clusters. *Chem. Commun.* **2010**, *46*, 7787−7789.

(47) (a) Palacios, M. A.; McLellan, R.; Beavers, C. M.; Teat, S. J.; Weihe, H.; Piligkos, S.; Dalgarno, S. J.; Brechin, E. K. Facile Interchange of 3d and 4f Ions in Single-Molecule Magnets: Stepwise Assembly of $[Mn_4]$, $[Mn_3Ln]$ and $[Mn_2Ln_2]$ Cages within Calix[4]-arene Scaffolds. *Chem. - Eur. J.* **2015**, *21*, 11212−11218. (b) Bag, P.; Chakraborty, A.; Rogez, G.; Chandrasekhar, V. Pentanuclear Heterometallic $\{Mn^{III}_2Ln_3\}$ (Ln = Gd, Dy, Tb, Ho) Assemblies in an Open-Book Type Structural Topology: Appearance of Slow Relaxation of Magnetization in the Dy(III) and Ho(III) Analogues. *Inorg. Chem.* **2014**, *53*, 6524−6533. (c) Cremades, E.; Gómez-Coca, S.; Aravena, D.; Alvarez, S.; Ruiz, E. Theoretical Study of Exchange Coupling in 3d-Gd Complexes: Large Magnetocaloric Effect Systems. *J. Am. Chem. Soc.* **2012**, *134*, 10532−10542. (d) Chandrasekhar, V.; Bag, P.; Kroener, W.; Gieb, K.; Müller, P. Pentanuclear Heterometallic $\{Ni_2Ln_3\}$ (Ln = Gd, Dy, Tb, Ho) Assemblies. Single-Molecule Magnet Behavior and Multistep Relaxation in the Dysprosium Derivative. *Inorg. Chem.* **2013**, *52*, 13078−13086.

(48) Rajaraman, G.; Totti, F.; Bencini, A.; Caneschi, A.; Sessoli, R.; Gatteschi, D. Density functional studies on the exchange interaction of a dinuclear Gd(iii)-Cu(ii) complex: method assessment, magnetic coupling mechanism and magneto-structural correlations. *Dalton Trans.* **2009**, 3153−3161.

(49) Barros, W. P.; Inglis, R.; Nichol, G. S.; Rajeshkumar, T.; Rajaraman, G.; Piligkos, S.; Stumpf, H. O.; Brechin, E. K. From antiferromagnetic to ferromagnetic exchange in a family of oxime-based MnIII dimers: a magneto-structural study. *Dalton Trans.* **2013**, *42*, 16510−16517.

(50) (a) Cirera, J.; Ruiz, E.; Alvarez, S.; Neese, F.; Kortus, J. How to Build Molecules with Large Magnetic Anisotropy. *Chem. - Eur. J.* **2009**, *15*, 4078−4087. (b) Maurice, R.; de Graaf, C.; Guihery, N. Magnetostructural relations from a combined ab initio and ligand field analysis for the nonintuitive zero-field splitting in Mn(III) complexes (vol. 133, 084307, 2010). *J. Chem. Phys.* **2010**, *133*, 084307−12. (c) Rajaraman, G.; Murugesu, M.; Sañudo, E. C.; Soler, M.; Wernsdorfer, W.; Helliwell, M.; Muryn, C.; Raftery, J.; Teat, S. J.; Christou, G.; Brechin, E. K. A Family of Manganese Rods: Syntheses, Structures, and Magnetic Properties. *J. Am. Chem. Soc.* **2004**, *126*, 15445−15457. (d) Sanz, S.; Frost, J. M.; Rajeshkumar, T.; Dalgarno, S. J.; Rajaraman, G.; Wernsdorfer, W.; Schnack, J.; Lusby, P. J.; Brechin, E. K. Combining Complementary Ligands into one Framework for the Construction of a Ferromagnetically Coupled $[Mn^{III}_{12}]$ Wheel. *Chem. - Eur. J.* **2014**, *20*, 3010−3013.

(51) (a) Hallmen, P. P.; Köppl, C.; Rauhut, G.; Stoll, H.; van Slageren, J. Fast and reliable ab initio calculation of crystal field splittings in lanthanide complexes. *J. Chem. Phys.* **2017**, *147*, 164101. (b) Rechkemmer, Y.; Fischer, J. E.; Marx, R.; Dörfel, M.; Neugebauer, P.; Horvath, S.; Gysler, M.; Brock-Nannestad, T.; Frey, W.; Reid, M. F.; van Slageren, J. Comprehensive Spectroscopic Determination of the Crystal Field Splitting in an Erbium Single-Ion Magnet. *J. Am. Chem. Soc.* **2015**, *137*, 13114−13120.

(52) Bhunia, A.; Gamer, M. T.; Ungur, L.; Chibotaru, L. F.; Powell, A. K.; Lan, Y.; Roesky, P. W.; Menges, F.; Riehn, C.; Niedner-Schatteburg, G. From a Dy(III) Single Molecule Magnet (SMM) to a Ferromagnetic [Mn(II)Dy(III)Mn(II)] Trinuclear Complex. *Inorg. Chem.* **2012**, *51*, 9589−9597.

DOI: 10.1021/acs.inorgchem.7b02608
Inorg. Chem. 2018, 57, 1158−1170